Variance Methods to Estimate Regional Heat Fluxes With Aircraft Measurements
in the Convective Boundary Layer

Ayumi Kotani* and Michiaki Sugita

Graduate School of Life and Environmental Sciences, University of Tsukuba
Tsukuba, Ibaraki 305-8572, Japan
phone/fax 81-29-853-6879
email: kotaniay@atm.geo.tsukuba.ac.jp and sugita@atm.geo.tsukuba.ac.jp

* corresponding author

Abstract

1

2

3

4

5   Turbulence data obtained by aircraft observations in the convective boundary layer (CBL) were analyzed to

6   estimate the regional surface heat fluxes through application of the variance methods.   Several heights

7   within and above the CBL were flown repeatedly above the flux observation site in a homogeneous steppe

8   region in Mongolia.   The vertical profiles of the second moment about the mean, i.e., the variance, of

9   temperature were found to follow in general the functional forms proposed in previous studies.   These

10   variance statistics were applied to the variance formulations to estimate surface sensible heat fluxes.   First,

11   the flux estimation was made with these equations and the constant parameters as proposed in previous

12   studies.   Then, the constants were re-calibrated with the current data set and used for flux estimation.   In

13   addition, a new simpler formulation was proposed and also calibrated with the current data set. Finally,

14   additional variables, which represent the large scale atmospheric conditions namely baroclinity and

15   advection, were considered for possible improvement of the flux estimation.   The resulting rms difference

16   of the estimated sensible heat flux and ground based measurements was reduced from about 40 - 100 Wm^{-2}

17   for the results obtained with the original constants and formulations, to 30 W m^{-2} or less for those obtained

18   with locally calibrated constants and introduction of four additional variables.   All formulations including

19   the new simple equation performed equally well.

20

21

22

23   Keywords: convective boundary layer, variance methods, surface fluxes, aircraft observations

24

1. Introduction

Knowledge of the fluxes of energy, mass and momentum between the land surfaces and the atmosphere is required in many situations encountered in water resource management and atmospheric circulation studies. Since the physical state of the convective boundary layer (CBL) probably reflects the surface fluxes with horizontal scales of the order of 10^2-10^5 m (e.g., Raupach and Finnigan, 1995), several approaches to derive surface fluxes with CBL observations have been developed and tested in the past. Examples of such approaches include the eddy correlation method (e.g., Lenschow et al., 1980), the profile or a bulk method of the CBL (e.g., Brutsaert and Sugita, 1991) and the CBL budget approach (e.g., Kustas and Brutsaert, 1987a, 1987b, Betts and Ball, 1994) with data obtained by sensors on a tower (e.g., Berger et al., 2001), on radiosondes (e.g., Sugita et al., 1999), aboard an aircraft (e.g., Lenschow et al., 1980), or by means of ground-based remote sensing devices such as Radar (e.g., Eng et al., 2003). Among them, aircraft measurements have the advantage in both detecting the spatial variability and in deriving area-averaged values depending on the methods applied to the measured variables, but they are not without disadvantages. The most notable feature is the random movement of an aircraft as a platform of observations. It continuously moves in all directions, and thus it requires simultaneous measurements of its precise position and also sophisticated and cumbersome treatment of the data afterward in order to allow vector data analysis, in particular for the application of the eddy correlation technique.

Methods to estimate surface fluxes from the associated variance measurements, on the other hand, are appealing particularly for the aircraft observation because they allow the derivation of surface fluxes only from measurements of a scalar variable without the need for extra measurements of aircraft position and data processing needed for the eddy correlation method as mentioned above. The variance methods are based on flux-variance relationships derived on the basis of similarity arguments and established through the determination of the constant parameters in the derived relationship. Such relations have been established and verified extensively through experiments in the surface layer and it now appears possible to derive surface fluxes with sufficient accuracy (e.g., Wesely, 1988; Katul et al., 1996). In contrast, for the CBL, the relevant flux-variance relationships are still not fully understood and far from established. So far the proposed functional relationships between the variances in the CBL and the corresponding surface fluxes are still limited in number and they have been insufficiently validated (see below). Also, they were used mainly for the purpose of organizing derived variances in terms of similarity functions, and only a few

studies have tried to apply such relations for the flux estimation. Sugita and Kawakubo (2003) used the variances of temperature in the lower half of the CBL obtained from tower observations to derive the surface sensible heat fluxes. There is only one study using aircraft data, namely the one by Asanuma (1996) and Asanuma and Brutsaert (1999), who used mixed and surface layer variance relations with temperature and humidity data obtained during HAPEX-Mobilhy (Hydrologic-Atmospheric Pilot Experiment and Modélisation du Bilan Hydrique) in southwestern France (André et al., 1986) to derive the corresponding surface fluxes.

In view of the lack of studies of the CBL variance relationships in general and their application for the surface flux estimation with aircraft data in particular, the present study was initiated with data sets obtained from an aircraft above an extensive steppe region in Mongolia with simultaneous surface flux observations, in order to investigate the CBL variance relationships and the feasibility to use them for the purpose of surface flux estimations of a region.

2. Methods

2.1 Experimental site

The temperature turbulence data in the CBL were obtained by aircraft observations that were carried out from June through October of 2003 as part of the field campaigns of the Rangelands Atmosphere-Hydrosphere-Biosphere Interaction Study Experiment in Northeastern Asia (RAISE, Sugita et al., 2006). The RAISE study area covers the Kherlen river basin in the northeastern part of Mongolia, where arid to semi-arid climate is dominant with a boreal forest in the northern and upper reaches of the watershed and steppe area towards the southern and downstream parts.

In this study, the data used for the analysis were taken above an extensive steppe region, where a flux observation station was operated as described below. The target area was located at and around a village called Kherlenbayan-Ulaan (47° 13′ N, 108° 44′ E, 1235 m ASL, to be referred to as KBU hereafter); its surface vegetation is comprised mainly of the cool-season C_3 species and a few C_4 species (Li et al., 2005) with their height around 0.2 m and leaf area index 0.5 at most, even at the peak growing season mainly because of the extensive grazing activities in this area (Sugita et al., 2006). The site was on a relatively flat terrace with horizontal extent of the order of 10^1 km along the Kherlen river (Fig. 1).

2.2 Aircraft observations

The instruments were installed on a wing of an aircraft (AN2), a single engine biplane, to measure the air temperature with a fine thermocouple whose time constant is rated as 0.4 s. The data were continuously sampled at 10Hz during the flight by a data logger (CR23X, Campbell Scientific Inc.). Positioning information was simultaneously obtained by a GPS receiver at 0.5 Hz and by a gyroscope that measured the angular velocity of the aircraft in the directions of its main body and the wing at 10 Hz intervals. Other measurements from the aircraft not directly used in the present study, included the absolute humidity by a Krypton hygrometer (KH-20, Campbell Scientific Inc.), the surface infrared temperature, incoming and outgoing shortwave radiation, and the spectral reflectance of the underlying surfaces in the range of 350-2500 nm.

As mentioned, the flight paths covered the KBU site and the surrounding area (Fig. 1) and flight levels of around 200, 500 and 1000m above the ground were flown repeatedly above this site. Although the lengths of the actual flight segments flown above the KBU site were slightly different one from another, depending on the weather condition and on the flight direction, only those flight segments longer than 5 km, which is equivalent to the averaging time of 100 s, and those whose standard deviation of the flight level was smaller than 50 m, were selected for analysis. Also, the data obtained in the June observations were found not to be usable for the present purpose because of data acquisition problems. This selection procedure produced 25 flight segments and data sets for the following analysis (Table 1).

To check the general reliability of the turbulence data, and also to check the scale of the turbulence observed, a Fourier transformation was applied to the measured time series listed in Table 1. The resulting power spectra, weighted by frequency, are shown in Fig. 2. The spectral peak frequency was found at around $f_p = 0.01$ Hz, and this corresponds to the length scale of 3 km, approximately, as the ground speed of the AN2 was around 30 m s^{-1}. Although the peak frequency and the general shape of the power spectra follow those reported in the literature (e.g., Kaimal and Finnigan, 1994), spectra attenuation can be observed in the inertial subrange at 0.1-1.0 Hz, as the slope is steeper than the commonly accepted value of -2/3. This might be due to the fact that the time constant of the temperature probe was not sufficiently small. Also, the power spectra exhibit a white noise in the higher frequency range above 1 Hz. A probable error in the variances due to this attenuation and to the white noise was estimated by calculating the difference between the ensemble mean spectra curve and a hypothetical curve obtained by assuming the slope of -2/3 in

1   the frequency range above f_p and of 1/1 below f_p.   It was found that the difference due to the attenuation and

2   to the white noise constitutes less than -8% and +3%, respectively, of the total variance in the range of 10^{-3} to

3   5 Hz.   In the present analysis, these are considered negligible and thus no correction was applied to the data

4   set before the analysis.   A possible impact of this procedure to the final results will be discussed below.

5   For each flight segment, the data were plotted as time series and checked visually.   They were then

6   further processed to remove a trend before the analysis by applying a linear regression method (Kaimal and

7   Finnigan, 1994); in brief, a linear equation $\hat{y} = ax + b$ was fitted to the measured temperature time series,

8   and all data were corrected by subtracting $\hat{y} - \bar{y}$ where $\bar{y}$ is the mean over the flight segment.   In most

9   cases, the correction was very small with the coefficient a in the range of -5×10^{-4} to 5×10^{-4} (K / 0.1s).   The

10 negative trend cases were usually caused by slight ascending motion of the aircraft during the flight segment.

11   The scale of the upwind surface source distribution of the observed temperature variances was evaluated

12 with the expression for scalar fluxes of Weil and Horst (1992), which was derived based on a CBL

13 Lagrangian stochastic dispersion model.   For an assumed mean wind speed $U = 10$ m s^{-1}, a CBL height h_i

14 = 1000 m, and a typical CBL velocity scale (see below) $w_* = 1.5$ m s^{-1}, this scale was found to be 0.6 km, 4.4

15 km, and 6.7 km, respectively for measurement heights of $z = 200, 500$, and 1000 m.   Note that portions of

16 some flight segments extend from general steppe area to the Kherlen river (Fig. 1); however, the results of

17 these segments were not markedly different from others and thus no separate treatments were made to these

18 data set.

19

20 **2.3 Ground based observation**

21

22   During the aircraft observations, the flux station at KBU site was in continuous operation.   The details

23 of the flux station have been presented in Li et al. (2005) and Sugita et al. (2006), but for the purpose of the

24 present study, use was made of the air temperature and wind velocity components measured at 10 Hz, and

25 the surface flux of the sensible heat H and the latent heat LE calculated by the eddy correlation method for

26 30 minutes.   Since the sums of H and LE were found to exhibit an energy imbalance in comparison with the

27 net radiation R_n and soil heat flux G, the energy shortage was distributed into the turbulence energy fluxes of

28 H and LE by keeping the Bowen ratio as suggested by Twine et al. (2000).   During the flight times, the

29 average closure ratio, $(H + LE)/(R_n + G)$ was 0.67, and the corrected H values ranged from 80 to 200 Wm^{-2}.

30 These corrected values were used as the reference surface fluxes and in what follows are referred to as H_s in

1   the case of the sensible heat flux and $\overline{w'\theta'}_s = H_s/(\rho c_p)$ in the covariance form in which w is the vertical

2   wind speed and θ *is* the potential temperature, ρ is the density of the air, and c_p is the specific heat at constant

3   pressure.

4

5   **2.4 Large scale meteorological data**

6

7   The outputs of a regional climate model (TERC- RAMS, Sato and Kimura, 2005) were used to evaluate

8   the mesoscale influence on the CBL variances through baroclinity and advection (see below).   The 6-hourly

9   NCEP/ NCAR reanalysis data set, which was produced for 2003 by essentially the same method described in

10   Kalnay et al. (1996), was used as the model forcing data to produce the downscaled (in time and space) data

11   set that includes the area and the intensive observation periods of the RAISE project (Sato et al., 2006).

12   This downscaled data set has a horizontal resolution of 30 km and a time interval of one hour.   However, in

13   this procedure, the atmospheric field within one grid of the 2.5˚ × 2.5˚ reanalysis data set was simulated by

14   the model without the inputs from observations and thus it is possible that a slight different in the cloud

15   formation or in the course of fronts and low pressure system could result in vastly different atmospheric and

16   surface condition at short time intervals.   For this reason, it is not appropriate to use instantaneous values of

17   these products at specific time and space.   Rather, they should be used as the time or space averages.   For

18   the baroclinity evaluation, the area of the size of 450×450 km^2 was adopted for space averaging, while for

19   the evaluation of the local horizontal advection, the 16 grids around the KBU site that cover an area of about

20   120×120 km^2 were used.   Both of them were further averaged in time over six hours, namely from 9 to 15

21   in Mongolian Daylight Saving Time (MDST=UT -9 hours).   Since aircraft observations were in general

22   carried out in clear sky condition without atmospheric disturbance such as the passage of the atmospheric

23   low system, the above averaging procedure should reduce or eliminate possible mismatch of the products

24   with actual conditions.   In fact, the same analysis was carried out with the space average over the same area

25   but without the time averaging.   The two data points nearest (in time) observation were interpolated to

26   derive instantaneous values at the time of observation.   The results turned out essentially the same as those

27   obtained with the time averages.   This is probably because of general steady condition of the atmosphere

28   during the flight observations.

29

30   **3. Results**

3.1 Variance profiles in the CBL

In order to assess the nature of the temperature variances obtained in the CBL over the experimental area, the observed variables were analysed based on a similarity theory. In the CBL, the main governing variables are the covariance of w and θ at the surface $\overline{w'\theta'}_0$, the buoyancy parameter g/θ with the gravity acceleration g, and the CBL height h_i, from which the convective scales can be organized. The first such proposal was made by Deardorff (1970), and the velocity scale w_* and the temperature scale T_* can be expressed as follows;

$$ w_* = \left[\overline{w'\theta'}_0 \left(g/\theta \right) h_i \right]^{1/3}, \ T_* = \frac{\overline{w'\theta'}_0}{w_*} = \left[\left(\overline{w'\theta'}_0 \right)^2 \left(g/\theta \right)^{-1} h_i^{-1} \right]^{1/3} \tag{1} $$

The convective scaling can usually be applied when the buoyancy driven turbulences are more dominant than the shear driven (i.e., mechanical) turbulences. One of the indices to indicate whether or not the convective scaling is applicable is $\mu = h_i / L$ where L stands for the Obukhov length, although the actual threshold value where the shear contribution becomes negligible depends on several factors such as the surface roughness (Asanuma, 1996). The range of μ in the data set used in this study was $16 \leq |\mu| \leq 550$, and this range in general indicates the dominance of the buoyant convection according to the previous studies (e.g., Wyngaard, 1985). However, since the judgement based on μ value has some ambiguity, there might still be a need for considering the surface shear effects. This can be accomplished by considering appropriate velocity scale, and possible choices are the friction velocity u_*, the convective velocity w_* for mechanical and convective scaling, respectively, and their combination such as $v_* = (w_*^3 + 8u_*^3)^{1/3}$ (Driedonks, 1982). Asanuma (1996) investigated the effects of the choice of the velocity scales on the variance formulation, and his results indicated that the choice had only a minor influence except for the u_* scaling which produced a worse result than the others. Thus, in this study, first both w_* and v_* were investigated, and at later part, based on the result of the first part, only the results with w_* will be shown.

The dimensionless values $\sigma_\theta^2 \, T_*^{-2}$ were plotted against $\xi = z h_i^{-1}$, where z is the sensor, i.e., aircraft height, as shown in Fig. 3. The value of h_i was estimated using a method proposed by Liu and Ohtaki (1997), with the peak frequency f_p of the spectra of the horizontal wind speed data obtained at the KBU flux station. Since it is not always easy to identify f_p from a single spectral curve, it was decided to evaluate f_p as the

1   average peak frequency of the six spectral curves.　In order to implement this procedure, six 55-min time

2   series were generated out of the raw turbulence data obtained over a 90-min period that included the time of

3   each flight segment.　Their power spectra were evaluated and then were used to derive the mean spectral

4   curve that was finally used to evaluate f_p for this flight segment.　Since it is quite possible to have errors of

5   around 100 m in the estimation of h_i with this procedure, and since it produces only a single value for the

6   selected 90-min period, the same h_i value was assigned to all flight segments within this 90-min period.

7   This is probably acceptable, since Sugita and Kawakubo (2003) reported that the CBL variance methods are

8   not very sensitive to the exact value of h_i.　It was found that h_i was around 700 – 1600 m during the flight

9   observation periods (Table 1).

10   In the past, several formulations have been proposed for the relationship between the scaled scalar

11   variance and ξ.　Among the first was Kaimal et al. (1976) who proposed (2) as a simple extension of the

12   surface layer variance equation under the free convective condition derived by Wyngaard et al. (1971) to the

13   CBL, by replacing L with h_i and $\theta_* \ (= -\overline{w'\theta'}_0 / u_*)$ with T_*

14

15
$$\frac{\sigma_\theta^{\ 2}}{T_*^2} = a\xi^{-2/3} \tag{2}$$

16

17   and they found (2) with $a=1.8$ predicted the measurements made by a tethered balloon in Minnesota well up

18   to the height of $0.1 \le \xi$.　Lenshow et al. (1980) also compared (2) with $a=1.8$ with the aircraft

19   measurements made over the East China Sea; Kaimal and Finnigan (1994) have noted that the observations

20   followed (2) in the range $0.1 \le \xi \le 0.5$, namely, the lower half of the CBL.

21   Based also on a convective scaling, a functional form (3) was proposed by Sorbjan (1989).　The major

22   difference is that he proposed to decompose the statistical variables in the CBL under the influence of

23   entrainment at the top of the CBL into a non-penetrative part (i.e., without the influence of entrainment) and

24   a residual part.　The non-penetrative part represents the diffusion from the ground surface, while the

25   residual part should take care of the entrainment flux.　His proposal applied to the temperature variance can

26   be written as

27

28
$$\frac{\sigma_\theta^{\ 2}}{T_*^2} = C_{M\theta_0} \frac{(1-\xi)^{4/3}}{\xi^{2/3}} + C_{M\theta_i} A_\theta^{4/3} \frac{\xi^{4/3}}{(1-\xi+D)^{2/3}} \tag{3}$$

9

where A_θ is the entrainment constant for heat flux defined as

$$\overline{w'\theta'}_h = -A_\theta \overline{w'\theta'}_0 \qquad (4)$$

where $\overline{w'\theta'}_h$ represents the flux at the CBL top, and A_θ has been found to take value in the range of 0.2-0.3 (e.g., Stull, 1976). The constants $C_{M\theta_0}$ and $C_{M\theta_i}$ were determined for $A_\theta = 0.2$ by Sorbjan (1989) by fitting (3) to the observations of Kaimal et al. (1976) and Caughey and Palmer (1979) although the exact procedure of the curve fitting was not explicitly stated; these values are listed in Table 2. The symbol D presents the ratio Δ / h_i with Δ being the depth of the interfacial layer at the top of the CBL, and its value was taken as zero in the present analysis partly because Sugita and Kawakubo (2003) have demonstrated that an introduction of D did not improve the estimation of fluxes, and mainly because D was not available for the present study. $A_\theta = 0.2$ was also assumed in the following analysis.

André et al. (1979) analysed the specific humidity gradient in the CBL with the idea to treat the turbulence statistics of a passive scalar in the CBL as a result of two independent diffusion processes, one originating up from the surface and another down from the capping inversion. This idea was further extended by Wyngaard and Brost (1984) as the so-called top-down and bottom-up (TDBU) model, and a version of the TDBU model for the scalar variance was derived by Moeng and Wyngaard (1984) and can be written as

$$\sigma_\theta^2 = \left(\frac{\overline{w'\theta'}_h}{w_*}\right)^2 f_t(\xi) + 2\left(\frac{\overline{w'\theta'}_h \, \overline{w'\theta'}_0}{w_*^2}\right) f_{tb}(\xi) + \left(\frac{\overline{w'\theta'}_0}{w_*}\right)^2 f_b(\xi) \qquad (5)$$

in which the symbols f_t, f_{tb} and f_b represent universal functions of ξ, which can be written as follows,

$$f_t = a_1(1-\xi)^{a_2}, \quad f_{tb} = a_3(1-\xi)^{a_4}\xi^{a_5}, \quad f_b = a_6\xi^{a_7} \qquad (6)$$

in which a_1 through a_7 are the constants determined empirically in Moeng and Wyngaard (1984) by fitting to the results obtained from the large eddy simulation and to the observations of Kaimal et al. (1976). Asanuma (1996) generalizes (5) by allowing the adaptation of different velocity scales at the inversion base

1   v_h and at the surface v_0 as follows;

2

$$\sigma_\theta^{\ 2} = \left(\frac{\overline{w'\theta'}_h}{v_h}\right)^2 f_t\left(\xi\right) + 2\left(\frac{\overline{w'\theta'}_h}{v_h}\frac{\overline{w'\theta'}_0}{v_0}\right) f_{tb}\left(\xi\right) + \left(\frac{\overline{w'\theta'}_0}{v_0}\right)^2 f_b\left(\xi\right) \qquad (7)$$

4

5   In this formulation, (5) can be seen as a special case of $v_h = v_0 = w_*$. As mentioned above, these scales could

6   include the effects of the surface shear and the convective forcing (i.e., buoyancy), and thus some

7   combinations including w_* and v_* were considered for v_h and v_0 in the following analysis. Since the velocity

8   was not directly measured by the aircraft in the present study, u_* was estimated by Rossby number similarity

9   which utilizes the geostrophic wind and the surface roughness z_0 as inputs. The detailed procedure to derive

10   z_0 and u_* values is described in the Appendix, but, briefly, z_0 around the target area was determined from the

11   topographic analysis as $z_0 = 0.054$ m and $z_0 = 0.430$ m for NW and SE directions, respectively. Since a

12   preliminary analysis indicated that the estimates of the sensible heat flux were not different by more than 1%

13   for both cases of z_0, only the results obtained with $z_0 = 0.430$ m are presented in what follows.

14   For the application of (7), the entrainment flux $\overline{w'\theta'}_h$ must also be expressed in terms of other

15   variables, since $\overline{w'\theta'}_h$ was not measured directly. In addition to (4), another model proposed by Tennekes

16   (1973) that includes both buoyancy (i.e., surface flux) driven and shear driven entrainment was considered.

17

18     $$\overline{w'\theta'}_h = -A\overline{w'\theta'}_0 - BT_a u_*^{\ 3}(gh_i)^{-1} \qquad (8)$$

19

20   Here A and B are constants and T_a is the air temperature. With those two models and the two velocity

21   scales, (7) was tested for three cases of i) $v_0 = v_h = w_*$ with (4), ii) $v_0 = v_*$, $v_h = w_*$ with (4), and iii) $v_0 = v_h = v_*$

22   with (8). The first case corresponds to the pure convective scaling, and (7) can be rewritten with (4) in a

23   similar format as (2)-(3) as follows and its functional form with the constants in (6) proposed by Moeng and

24   Wyngaard (1984) is shown in Fig. 3.

25

26     $$\frac{\sigma_\theta^{\ 2}}{T_*^2} = A_\theta^{\ 2} f_t\left(\xi\right) + 2A_\theta f_{tb}\left(\xi\right) + f_b\left(\xi\right) \qquad (9)$$

27

28   For the other two cases, Asanuma (1996) derived the constants in (6) with data from the aircraft observation.

1   Sugita and Kawakubo (2003) also determined these constants with the data obtained from the tower

2   observation by optimising the constants to minimize the error of flux evaluation.   These coefficients are

3   listed in Table 2 for each case.

4   Fig. 3 indicates that the observed variance values follow in general the proposed functional forms,

5   except in the upper parts of the CBL, where the scatter becomes larger probably because of the entrainment

6   flux that becomes dominant near the inversion layer.   Since the depth of the inversion layer can be as large

7   as about 40% of that of the CBL (Stull, 1988) and there are some uncertainties remaining in the estimated

8   values of h_i, the values registered as just below h_i could actually have been above the CBL or within the

9   inversion layer.   Thus, it was decided not to use the four data sets obtained at heights above $0.8h_i$ for the

10   purpose of estimating fluxes.

11

12   **3.2 Application of Variance Methods in the CBL for Flux Estimation**

13

14   Equations (2) and (3) with $D = 0$ can be recast to obtain the surface flux $\overline{w'\theta'}_0$ as

15

16
$$\overline{w'\theta'}_0 = \sigma_\theta^{3/2} \left[\frac{gh_i}{\theta}\right]^{1/2} \left(a\xi^{-2/3}\right)^{-3/4} = \sigma_\theta^{3/2} \left[\frac{gz}{\theta}\right]^{1/2} a^{-3/4} \tag{10}$$

17
$$\overline{w'\theta'}_0 = \sigma_\theta^{3/2} \left[\frac{gh_i}{\theta}\right]^{1/2} \left[C_{M\theta_0} \frac{(1-\xi)^{4/3}}{\xi^{2/3}} + C_{M\theta_i} A_\theta^{4/3} \frac{\xi^{4/3}}{(1-\xi)^{2/3}}\right]^{-3/4}. \tag{11}$$

18

19   Similarly, the TDBU formulation (7) can be rewritten as follows,

20

21
$$\overline{w'\theta'}_0 = \sigma_\theta \left[\frac{A_\theta^2}{v_h^2} f_t(\xi) - 2\frac{A_\theta}{v_h v_0} f_{tb}(\xi) + \frac{1}{v_0} f_b(\xi)\right]^{-1/2} \tag{12}$$

22

23   For cases i), i.e., $v_0 = v_h = w_*$ with (4), this can easily be solved to obtain $\overline{w'\theta'}_0$ from σ_θ.   However, for the

24   other two cases of ii) and iii), (12) becomes an implicit function for $\overline{w'\theta'}_0$.   Thus, an iteration procedure is

25   required to solve (12).   This was carried out as follows.   First, $\overline{w'\theta'}_0 = \overline{w'\theta'}_s$ was assumed in the right

26   hand side (RHS) of (12), and this produced the first estimate of $\overline{w'\theta'}_0$.   Then this value was inserted in the

27   RHS of (12) and the second estimate was derived.   This process was repeated until $\overline{w'\theta'}_0$ value had

12

1   converged sufficiently.　Note that the choice of the first estimate is not really relevant since the choice of the

2   twice and 1/2 of $\overline{w'\theta'}_s$ as $\overline{w'\theta'}_0$ resulted in the same final value. In what follows, surface fluxes derived

3   by means of the variance methods will be denoted as $\overline{w'\theta'}_{vm}$.

4   As mentioned, the constants in these equations are still not well established.　As such, in the present

5   analysis, first, the constants proposed in previous studies were tested, and, then, they were calibrated with the

6   current data sets. The calibration was performed in the same manner as in Sugita and Kawakubo (2003),

7   where the constants were changed in small steps until the root mean square (rms) difference between

8    $\overline{w'\theta'}_{vm}$ and $\overline{w'\theta'}_s$ reached a minimum.　For the TDBU formulation, the powers of (6) were retained and

9   only the others were changed.

10   These results are shown graphically in panel (a) and (b) of Figs. 4-8, and the calibrated constants and

11   relevant statistics are listed in Table 2 and Table 3, respectively.　Figs. 7-8 and Table 3 indicate that the

12   cases ii) and iii) of (7) in which v_* was assigned as the relevant velocity scale resulted in a large rms

13   difference.　This is particularly evident in case ii) with the original constants from the literature were used.

14   In order to assess the cause of the large rms difference, a simple sensitivity test for flux estimation was

15   carried out.　For a typical condition of $\theta = 300$ K, $u_* = 0.25$ m s^{-1} and $\overline{w'\theta'}_s = 0.15$ K m s^{-1}, σ_θ was changed

16   ± 0.1K from 0.15K and the resulting changes of $\overline{w'\theta'}_{vm}$ were examined.　The result is shown graphically

17   in Fig. 9 for the cases i), ii) and iii) of (7) with the constants calibrated with the current data set.　Note that

18   for the case i), a formal error analysis can also be made, and it is presented with others at later part of this

19   paper.　It can be seen that the estimated flux is quite sensitive to σ_θ at around the middle to higher portions

20   of CBL, which means that data with the same level of accuracy but observed at levels with higher sensitivity

21   could produce a worse result.　Indeed the poor agreements between $\overline{w'\theta'}_{vm}$ and $\overline{w'\theta'}_s$ were obtained for

22   the data observed at these heights.　Thus it is probable that the small measurement error in σ_θ measurements

23   at heights where the functional forms have higher sensitivity has caused larger rms error.

24   As can be seen from the figures and Table 3, the rms difference was reduced from more than 4×10^{-2} K m

25   s^{-1} to 3-4$\times10^{-2}$ K m s^{-1} by adjusting the constants through the calibration (panel (b)).　This implies that these

26   experimental constants indeed contain uncertainty as mentioned above.　However, this need for the

27   calibration may have arisen from the 8% underestimation and 3% overestimation of the variance that were

28   caused by respectively the slow response sensor and the white noise as mentioned above.　However, this is

29   not clearly the case as can easily be shown from a simple error analysis of the variance and the flux as

30   follows.　The rms difference of the σ_θ^2 values between those from the observations and those predicted by

1   (2), (3) and (5) with the original constants is 1.1-1.9×10^{-2} K^2. This is order of magnitude larger than the

2   difference that can be accounted for by the measurement error alone, as the mean σ_θ^2 value is 1.6×10^{-2} K^2

3   and thus the 8% underestimation of σ_θ^2 can be translated into the underestimation of 1.0×10^{-3} K^2 and the 3%

4   overestimation of σ_θ^2 into that of 0.5×10^{-3} K^2. Similarly, from the view point of flux evaluation, since

5   $\overline{w'\theta'}_0$ is proportional to $\sigma_\theta^{3/2} = (\sigma_\theta^2)^{3/4}$, the 5% underestimation of σ_θ^2 corresponds to 4% underestimation

6   in flux; this is an order of magnitude smaller than the reduced rms difference of around 30% by the

7   calibration. Thus the measurements error is probably of lesser importance to the fact that the local

8   calibration was necessary.

9   The data points for (10) in the height range of $z > 0.5h_i$ were also drawn in Fig. 4, even though (10) was

10   derived originally only for the lower parts of CBL. In the calibration and the calculation of the statistics,

11   only the data obtained below $0.5h_i$ were used. Thus, it is not surprising that even after the calibration of the

12   empirical constants, the outlier points remained. However, the calibration with all data for $z < 0.8h_i$ was

13   also carried out, and it was found that the result is not markedly different from the case with data for $z < 0.5h_i$.

14   This tends to indicate that the flux is not very sensitive to the exact value of σ_θ at higher levels in the CBL.

15   However, a simple error propagation analysis (see below) of (10) has indicated that the sensitivity of fluxes

16   to the error of σ_θ measurement is actually lower near the surface and increases as z increases toward h_i.

17   Thus the agreement found for the data at higher elevations may due to the lack of strong influence of the

18   entrainment with the current data set, and, in general, (10) may still be better used for $z < 0.5h_i$.

19   Since it is the treatment of the entrainment that makes relevant equations (11) and (12) more complex

20   with variables difficult or even practically impossible to obtain, it is of some interest to make a simpler

21   equation such as (10) but that allows prediction of the increase of σ_θ^2 at higher levels in the CBL near $z = h_i$.

22   One of such simple functions can be expressed as

23

24
$$\frac{\sigma_\theta^2}{T_*^2} = b_1 \xi^{-2/3} + b_2 \left(b_3 - \xi \right)^{b_4} \tag{13}$$

25

26   and in the flux-variance relation form,

27

28
$$\overline{w'\theta'}_0 = \sigma_\theta^{3/2} \left[\frac{gh_i}{\theta} \right]^{1/2} \left[b_1 \xi^{-2/3} + b_2 \left(b_3 - \xi \right)^{b_4} \right]^{-3/4}. \tag{14}$$

14

This formulation is based on a similar idea to the TDBU or that of Sorbjan's with the superposition of the two diffusion processes, one from the surface and one from the CBL top, but unlike their formulations, the relevant variable is ξ only.

This formulation was tested by determining the constants b_1 through b_4 as follows. First, several combinations of these constants that produced the smallest rms difference between the calculated and reference fluxes, were selected by the same manner described above. Such combinations are not necessarily unique and indeed in the case of (14) several choices were possible. Among them, the combination that allow predictions of $\sigma_\theta^2 T_*^{-2}$ which agrees with those by (9) for $z > 0.8 h_i$ was finally selected. In another word, constants were selected in such a way that allows (13) to simulate the effect of the entrainment in the upper layer as expressed by (9). The resulting constants were used in (14) to derive fluxes, and were compared with the reference fluxes. As can be seen from Table 3, the rms difference is very close to that of the more complex formulations such as (11) and (12). Yet, unlike (10), (14) should work equally well with (11) or (12) at higher range of $z > 0.8 h_i$, and thus could be advantageous for practical applications of the variance methods. Further studies should be carried out to study whether or not the same constants b_1 through b_4 can also be used with other data sets.

The above analysis has indicated that the local calibration of the constants improved the performance of (10)- (12) in the context of flux estimation. However, the scatter still exists. This might possibly be reduced with an introduction of additional variable parameters. As mentioned, up to now it has been assumed that the relevant variables for CBL variances are z, h_i and $\overline{w'\theta'}_0$. However, it is quite possible that other variables may play a role. For example, for the study of profiles or bulk formulation in the CBL, several variables whose effect is not negligible have been identified. These variables include the Coriolis parameter f, the Ekman layer depth $h_r = \kappa\, u_* f^{-1}$ where κ is a constant, the vertical gradient of geostrophic wind i.e., baroclinity, $\partial U_g/\partial z$, $\partial V_g/\partial z$, and the horizontal gradient of advection $\partial(u\theta)/\partial x$, $\partial(v\theta)/\partial y$ in which u and v are wind speed components in the northward and eastward direction, respectively. The vertical gradients of U_g and V_g can be expressed in terms of horizontal gradients of temperature, that is, by the thermal wind relation to a good approximation,

$$\frac{\partial U_g}{\partial z} = -\frac{g}{fT}\frac{\partial T}{\partial y}, \quad \frac{\partial V_g}{\partial z} = \frac{g}{fT}\frac{\partial T}{\partial x}. \tag{15}$$

These additional variables were evaluated with the outputs of the regional climate model as described before.

These variables can be organized to form several non-dimensional variable parameters. With three basic dimensions of length, time and temperature and eight independent variables, five independent dimensionless variable parameters can be created by following Brutsaert and Mawdsley (1976), who discussed the variables in relation to the mean profiles of the CBL,

$$\xi = z / h_i \tag{16}$$

$$\mu = h_i / L \tag{17}$$

$$\nu = h_i / h_r \tag{18}$$

$$\beta_x = \frac{\partial u_g}{\partial z}\left(\frac{h_i}{h_r}\right)^2 \frac{1}{|f|}, \beta_y = \frac{\partial v_g}{\partial z}\left(\frac{h_i}{h_r}\right)^2 \frac{1}{|f|}, \beta = \left(\beta_x{}^2 + \beta_y{}^2\right)^{1/2}. \tag{19}$$

In a similar manner, the advection term can be made dimensionless as follows:

$$\gamma_x = \frac{\partial \overline{u\theta}}{\partial x}\frac{h_i}{\overline{w'\theta'}_0}, \gamma_y = \frac{\partial \overline{v\theta}}{\partial y}\frac{h_i}{\overline{w'\theta'}_0}, \gamma = \left(\gamma_x{}^2 + \gamma_y{}^2\right)^{1/2}. \tag{20}$$

The non-dimensional variables γ and β include two horizontal components, and thus it is possible to treat them either as the combined variable or as independent variables of γ_x and γ_y, and β_x and β_y, and both cases were tested in what follows. The actual values of each non-dimensional variable parameter determined for the study area are listed in Table 4. For the TDBU formulation, since the inclusion of v_* as scaling parameter resulted in less accurate result as shown above, only the case with w_* scaling, i.e., (9), was considered hereafter.

Among those dimensionless variables, ξ had already been included in the variance profile formulations (2), (3), (9) and (13). Therefore other four variables were added linearly as follows,

$$\left(\frac{\sigma_\theta}{T_*}\right)^2 = F\left(\xi\right) + c_1\mu^{c_2} + c_3\nu^{c_4} + c_5\beta^{c_6} + c_7\gamma^{c_8} + c_9 \tag{21}$$

where F is a function of ξ, which can be taken as the RHS of one of (2), (3), (9) or (13). The equation can be rewritten for $\overline{w'\theta'}_0$ as

$$\overline{w'\theta'}_0 = \sigma_\theta^{3/2} \left(\frac{g}{\theta} h_i \right)^{1/2} \left[F(\xi) + c_1\mu^{c_2} + c_3\nu^{c_4} + c_5\beta^{c_6} + c_7\gamma^{c_8} + c_9 \right]^{-3/4} \tag{22}$$

and the coefficients c_1 through c_9 were determined to minimize the rms difference between $\overline{w'\theta'}_0$ and $\overline{w'\theta'}_s$. Note that when γ is considered, (22) becomes implicit, and thus an iteration is required to determine $\overline{w'\theta'}_0$. This was carried out in the same manner to solve (12); an initial value of $\overline{w'\theta'}_0 = \overline{w'\theta'}_s$ was first inserted into the RHS of (22), and the resulting value of $\overline{w'\theta'}_0$ from (22) was again inserted into the RHS of (22). This was repeated until the value of $\overline{w'\theta'}_0$ had sufficiently been converged. Just like the case of (12), the final value is not sensitive to the choice of the initial value. Note also that possible other functional forms other than (21) were also tested since there is no a priori reason that these additional non-dimensional variables should be organized as a linear function. Since there is no theory or study that helps to organize a proper functional form, some arbitrary forms were tested. They included a product of the variables and a linear function of log of these variables, among some others. However, the result was not very different from the one obtained by (22) and thus only the result with (22) will be shown. It is not clear if this is because the number of the data points is not sufficient to produce meaningful difference among the different functional forms or the process of the calibration took care of the difference of the formulation.

The results are shown in panel (c) of Figs. 4-6 and in Tables 2 and 3. Clearly, the inclusion of the additional variables has successfully reduced the rms difference. To investigate which variable(s) have more contribution for the improvement of accuracy of the flux estimation, all possible combinations of the variables were tested, and this result is shown in Fig 10. It can be seen that in general the rms difference decreases as the number of variable parameters increases. In the case of addition of one parameter, β (and especially their y component) are slightly more effective to reduce the rms difference than the others, although the difference is not statistically significant at the 5% level, and it becomes unclear as the number of the additional variables increased. It was also found that the rms differences of the fluxes with (19) and (20) for the separate treatment of the x- and y-component and for the combined expressions are different by only a few W m^{-2}. This is probably because the horizontal gradient of the wind and temperature fields in the atmosphere around the experimental area are more or less the same during the flights and thus it is the

1   magnitude and not the direction of β that counted.   Naturally in different settings, it is quite possible that the

2   separate treatment works better.

3   As a whole, the rms differences reduced to about 3×10^{-2} - 4×10^{-2} K m s^{-1} which roughly correspond to H

4   = 30 to 40 W m^{-2}, after the calibration of the constants, and further down to 3×10^{-2} K m s^{-1} (H = 30 W m^{-2}) or

5   less with the introduction of the additional dimensionless variables.   The reduction of the rms error from the

6   result with the original formulations to that with (22) was found significant at the 5% significant level except

7   for (2), for which it is significant only at the 10% level.   The difference among the results with different

8   formulation of (2), (3), (7) and (13) was not found significant even at the 10% level.   In another word, the

9   same level of agreement was obtained by all formulations.   This is partly due to the fact that a local

10 calibration was carried out.   Thus as long as the calibration is possible, the simplest form, i.e., (22) with

11 (13) that covers the whole CBL may be a good choice from a practical point of view.

12   Finally, it is important to discuss why the local calibration was found needed in the CBL variance

13 methods, and also to identify where the sources of the remaining estimation error of H of around 30 W m^{-2}

14 are even after the calibration and the introduction of the additional variables.   There are several possibilities

15 for the first question, but main reasons probably consist of (i) the difference of the optimization target, (ii)

16 the difference in the method of deriving reference fluxes, (iii) random error of the H derived by the variance

17 formulation as a result of error propagation of the measurement error, (iv) measurement error of the reference

18 H values, (v) the sampling error of measured σ_θ, and (vi) insufficient treatment of physics in the

19 formulations.

20   The above possibilities (i)-(ii) are relevant mainly for the first question, while (iii)-(iv) are probably for

21 the second question.   The issues (v)-(vi) apply both questions.   The earlier studies focused their analysis to

22 optimize the constants to produce the best agreement of σ_θ^2, while only in later studies the agreement of H

23 was targeted.   Since the equations are non-linear, this difference could result in different sets of constants.

24 For the second point, the reference H values were obtained in this study by the eddy correlation method and

25 corrected to ensure the energy balance closure.   Earlier studies to have optimized flux estimation did not

26 apply this type of correction.   For example, in Sugita and Kawakubo (2003), the reference fluxes were

27 determined through the linear extrapolation of H measured at 3-4 levels in the height range of 25-200 m

28 down to the surface.   No attempt was made to make energy balance closure.   Since $\overline{w'\theta'}_s / \overline{w'\theta'}_{vm} <1.0$

29 (Table 3) was obtained with the constants of Sugita and Kawakubo (2003), and since the correction of the

30 energy imbalance usually brings H larger, this different treatment of the energy balance closure issue could

1 be one of the reasons for the need of the local calibration.

2 The formulations of the variance methods should produce H with some error, even if the formulations

3 were perfect with all relevant physics incorporated.   This is because inputs data have some measurements

4 error and they are propagated into the final results.   This can be assessed by a simple error analysis.   An

5 error propagation equation for the variance methods can be expressed as,

6

7
$$\delta\overline{w'\theta'}_0 = \left[\left(\frac{\partial\overline{w'\theta'}_0}{\partial\sigma_\theta}\delta\sigma_\theta\right)^2 + \left(\frac{\partial\overline{w'\theta'}_0}{\partial\xi}\delta\xi\right)^2 + \left(\frac{\partial\overline{w'\theta'}_0}{\partial P_i}\delta P_i\right)^2 + \text{L}\right]^{1/2} \qquad (23)$$

8

9 where the symbol δ represents the absolute error, and P_i is the i-th additional variable, i.e., one of the second

10 through sixth term of (21).   A preliminary analysis indicated that the value of $\dfrac{\partial\overline{w'\theta'}_0}{\partial\sigma_\theta}\delta\sigma_\theta$ was one to

11 two-order larger than the other terms, and thus all terms containing P_i were added to produce a single term

12 expressed as δP in the following analysis.   Those results for (22) with (10), (11), case i) of (12) and (14)

13 for $\theta = 300\text{K}$, $\sigma_\theta = 0.15\text{K}$, $h_i = 1000\text{m}$, $P = 0.5$, $\delta\sigma_\theta = 0.1\text{K}$, $\delta P = 0.5$, and $\delta\xi = 0.1$ are plotted against ξ in

14 Fig. 9.   It can be seen that the possible error can be as large as 0.1-0.2 for the above condition and has the

15 maximum at around $\xi=0.5$ for (22) with (11), (12) and (14), and at $\xi=1$ for (22) with (10), and thus it is

16 possible that measurement error of σ_θ observed near the mid altitude contributed part of the remaining rms

17 difference.   As indicated in Table 1, most of the measurements were made in the height range of $0.2<\xi<0.5$.

18 In the future application, it can be recommended that the observation should be made in the heights around

19 $\xi=0.2\text{-}0.3$ or $\xi=0.7\text{-}0.8$ to obtain results with smaller errors for the same type of instruments, although in

20 practice it is not necessarily easy to know the exact value of h_i and hence ξ during flights.   Note also that

21 Fig.9 indicates that the magnitude of error of each equation is about the same except for (22) with (10), and

22 thus, from the viewpoint of error reduction, there is not an advantage to choose a particular formulation.

23 For the fifth point, it is always possible for the measured value of σ_θ^2 to be underestimated with some

24 random error as it is measured for a finite length of time, while with outputs of LES, this may not necessarily

25 be the case.   The data of insufficient length in general should cause underestimation as they may not contain

26 fluctuations of larger scales, and, according to Lenschow et al. (1994), it can be separated into the systematic

27 and the random errors.   The systematic error is the difference between the true, theoretical variance σ_θ^2

1 obtainable by taking infinite observation length and the ensemble average of sampled σ_θ^2 for the averaging

2 length L_θ, i.e., $<\sigma_\theta^2(L_\theta)>$ and can be expressed as (24) (Lenschow et al., 1994), after their notation with time

3 is changed into that with length,

4

$$\frac{\sigma_\theta^2 - \left\langle \sigma_\theta^2 (L_\theta) \right\rangle}{\sigma_\theta^2} \approx 2 \frac{\lambda_\theta}{L_\theta} \qquad (24)$$

6

7 in which $< >$ indicates the ensemble average, λ_θ is the integral length scale of σ_θ. Similarly, the random

8 error is the difference between σ_θ^2 evaluated for L_θ and its ensemble average $<\sigma_\theta^2(L_\theta)>$, and can be

9 expressed by,

10

$$\frac{\left\langle \left| \sigma_\theta^2 (L_\theta) - \left\langle \sigma_\theta^2 (L_\theta) \right\rangle \right| \right\rangle}{\sigma_\theta^2} \approx \left(4.1 \frac{\lambda_\theta}{L_\theta} \right)^{1/2} \qquad (25)$$

12

13 Both errors can easily be determined once λ_θ has been known. This was estimated by an empirical function

14 of Lenschow and Stankov (1986),

15

$$\lambda_\theta = h_i \xi^{1/2} . \qquad (26)$$

17

18 For the present flight segments, they produce values in the range from 8% to 31% with the average of 16%

19 for the systematic error and 40% to 70% with the average of 55% for the random error for estimating σ_θ^2.

20 To suppress an underestimation due to the systematic and random errors down to a level of 10%, it is

21 required that the flight segment satisfies $L_\theta \geq$ 14 km and $L_\theta \geq$ 295 km with h_i = 1000 m and z = 500 m for

22 the systematic and random error, respectively. In practice, although it is not easy to satisfy such

23 requirements, it is still a good idea to make sequential flights over the same track at the same level to

24 increase L_θ (Sun and Mahrt, 1994).

25 For the sixth point of the possible problem of the variance methods, it is quite possible that there

26 are some relevant physics not sufficiently incorporated within the variance formulations. However, it is not

27 clear at this point whether this is the case, since other factors mentioned above could very well have

28 dominated the remaining error and introduction of the other parameters or formulations may not have

29 sufficient impacts on to the final results. This is partially true with the introduction of the larger scale

atmospheric variables that have been achieved in this study.   Clearly more studies with a better data set are needed to fully answer this question.

4. Conclusions

Turbulence data obtained by aircraft observations in the CBL over an extensive steppe region in Mongolia were analysed to estimate the surface fluxes by means of CBL variance methods.   Observed temperature variances were found to follow, in general, the functional forms proposed in the past for $\sigma_\theta^2\, T_*^{-2}$ in the CBL, i.e., (2), (3) and (7).   The same functions in a different form namely (10), (11) and (12) were then used for the estimation of $\overline{w'\theta'}_0$ from measured σ_θ^2 values.   With the functional forms and the original constants listed in Table 2, this procedure produced $\overline{w'\theta'}_0$ values that agree with the reference fluxes measured at the KBU flux station with a rms difference of about 40 to 100 Wm^{-2}.   After calibration of the constants in (10), (11) and (12) with the current data set, the same procedure yielded the fluxes with a rms difference of 30 to 40Wm^{-2}.   After inclusion of the additional variable parameters, (17)-(20), which represent the large scale atmospheric influence, and calibration of the constants in (22), the rms difference was further reduced down to about 30 Wm^{-2} or less.

For the more complicated and physically based formulation of (7), several options are available in choosing velocity scales.   The results have indicated, however, that the convective scaling velocity w_* produced always better results than the u_* scaling, and this partly agrees with the result obtained by Asanuma (1996).   It appears that u_* is totally irrelevant in the turbulence characteristics of temperature within the CBL.   This in turn means that there is no clear advantage to use (7) or (12) because of their flexibility in choosing different velocity scales.   Also, the comparison of the fluxes has shown that all formulations, (10), (11) and (12), are capable of producing $\overline{w'\theta'}_0$ at the same level of accuracy, except perhaps for (10), because of the lack of consideration of the entrainment in this formulation, for data at higher elevation. From the view point of the sensitivity of the resulting $\overline{w'\theta'}_0$ from each formulation to the measurement error of σ_θ^2, a simple error propagation analysis has shown that all formulations give the same level of sensitivity with larger sensitivity near the middle of CBL, except again for (10) which shows higher sensitivity than the others at higher elevation.   This also indicates that there is no clear reason to choose one particular formulation.   One advantage, however, to use more complex formulations of (11) and (12) is that

1 they cover whole height range of ξ. In order to allow use of a simple equation that covers whole height

2 range, (14) was proposed. Unlike (10), the usage can extend to the height under the influence of

3 entrainment at a similar accuracy as (12), is capable of producing fluxes with the same level of accuracy, has

4 the same sensitivity to the measurement error of σ_θ^2, and yet is a function of ξ only. For practical

5 applications, (14) probably serves better than the others, at least until all the needed data such as D in (3)

6 become available for a complete test of more physically based equations.

7   Finally, the present analysis has indicated that the CBL variance methods with data obtained by aircraft

8 are capable of producing surface fluxes. However, two major issues among others remain not completely

9 solved. First, the local calibration of the constants in the CBL variance equations was found needed to

10 achieve flux estimation with sufficient accuracy. It is not very clear at this point whether or not the need of

11 the local calibration is an indication of the lack of universality of the equations, given the wide range of data

12 sets employed in the past and their uncertainties. Second, even after the inclusion of the additional

13 non-dimensional variable parameters that indicate the large scale influence to the CBL properties, there

14 remained a difference between $\overline{w'\theta'}_0$ values estimated from the variance methods and those from the flux

15 station. Again, it is not clear if this is because of a problem inherent in the variance formulations where

16 relevant physics may not be completely incorporated or because of measurement problems, although several

17 possibilities such as the sampling issue were identified. Clearly more studies are needed to answer these

18 questions.

19

20

21

Appendix: Derivation of friction velocity at regional scale

Since velocity was not directly measured by the aircraft in the present study, u_* was estimated from a formulation based on Rossby-number similarity which relates the surface stresses and the geostrophic wind (e.g., Zilitinkevich, 1975),

$$\frac{u_*^2}{G^2} = k^2 \left\{ \left[\ln\left(\frac{u_*}{|f| z_0}\right) - A \right]^2 + B^2 \right\}^{-1} \qquad (A-1)$$

where G is the geostrophic wind, f is the Coriolis parameter, k is von Kármán's constant, and z_0 is the surface roughness length. The symbols A and B represent universal functions of the stability h_i / L where L is the Obukhov length, and those proposed by Zilitinkevich (1975) were adopted in the analysis. The northward and eastward components of G, i.e., U_g and V_g, were evaluated from the pressure gradient on a 750 hPa isobaric surface from the outputs of the regional climate model as described above. The value of z_0 was estimated from the formulation of Grant and Mason (1990), (A-2), which is based on the idea that the total stress at a particular height should be the sum of the form drag on major roughness elements such as topography and the shear stress acting on the local surface,

$$\frac{z_0}{h} = \frac{1}{2} \left(\exp \left\langle \frac{k}{\left\{ \lambda D_{h/2} + k^2 \left[\ln\left(h / 2 z_{0l}\right) \right]^{-2} \right\}^{1/2}} \right\rangle \right)^{-1} \qquad (A-2)$$

where h is the mean height of the major obstacles, $\lambda = A / S$ is the roughness density with A being the silhouette area of the roughness elements on a horizontal area S, $D_{h/2}$ is the drag coefficient of the major obstacles evaluated at $z = h/2$ and z_{0l} is the local roughness length of the surface. To apply (A-2), $D_{h/2}$ and z_{0l} must be known. The drag coefficient $D_{h/2}$ was evaluated from an expression of Lettau (1969), which was derived from an experiment with bushel baskets placed in different arrays on an icy lake surface,

$$\frac{z_0}{h} = c\lambda \qquad\qquad (A\text{-}3)$$

where c is a constant (≈ 0.5). The z_0 value of (A-3) in his experiment was mostly from the major obstacles of the baskets and the contribution from the shear stress of the icy surface itself was probably minimal, and thus can be used to estimate $D_{h/2}$ in (A-2). Once z_0 has been evaluated from (A-3), it can be converted to the drag coefficient $D_{h/2}$ as follows. The form drag F can be given as

$$F = D_{h/2}\rho A u_{h/2}^2 \qquad\qquad (A\text{-}4)$$

where $u_{h/2}$ is the wind speed at $z=h/2$. The wind profile equation in surface layer derived from Monin-Obukhov similarity theory (e.g., Brutsaert, 1982), on the other hand, can be given as,

$$u = \frac{u_*}{k}\left[\ln\left(\frac{z-d_0}{z_0}\right) - \Psi_m\left(\frac{z-d_0}{L}\right)\right] \qquad\qquad (A\text{-}5)$$

where Ψ_m is the stability correction function for momentum with Obukhov length L. By assuming neutral stability ($\Psi_m = 0$), neglecting the regional scale displacement height d_0, and by noting $\tau = \rho u_*^2 = F / S$, one can rewrite (A-4) as

$$\lambda D_{h/2} = k^2\left[\ln\left(\frac{h}{2z_0}\right)\right]^{-2} \qquad\qquad (A\text{-}6)$$

which allows a conversion from z_0 estimated by (A-3) to $D_{h/2}$ to be used in (A-2).

For the actual application, first, λ of the target area was evaluated. Although the original definition of λ is the areal density, it is not straightforward to determine λ from topographic information. Thus, the streamwise density (Kustas and Brutsaert, 1986; Sugita and Brutsaert, 1990; Hiyama et al., 1996) was used instead in the present analysis, and it was estimated by applying,

$$\lambda = \frac{\sum\limits_{i=1}^{n} y_i}{\sum\limits_{i=1}^{n} \delta_i} = \frac{\sum\limits_{i=1}^{n} y_i}{X} \qquad (A-7)$$

where y_i is the height of the ith roughness obstacle, δ_i is the distance between the i-th and $(i-1)$th obstacle along the line, and X is the length of the cross-sectional line. To obtain cross sections, two 10-km lines from the KBU site in the major flight directions of respectively, NW and SE were established and terrain profiles were derived from a DEM data set with a horizontal resolution of 7-12.5 m and a vertical resolution of 15 m, produced as part of ASTER 3D data set (Abrams, 2000). The value of y_i is taken as the height of the windward side of the obstacles and used in Eq. (A-7) to derive the value of λ.

The local roughness length z_{0l} was estimated by means of (A-5) with the data sets of u_*, u, H and LE measured at the KBU flux station by assuming $d_0/h = 2/3$. The resulting z_{0l} value was found to be in the range of 10^{-2} to 10^{-4} m during the observation periods. Since there was no clear seasonal trend observed in the derived z_{0l} values, a logarithmic mean value $z_{0l} = 0.003$ m was used in what follows. With these values of $D_{h/2}$ and z_{0l}, the roughness length of the area was determined from (A-2) as $z_0 = 0.054$ m and $z_0 = 0.430$ m for NW and SE directions, respectively. The larger roughness of the SE direction was due to the presence of a hilly area as can be seen in Fig.1. With the derived z_0 value, u_* values were evaluated from (A-1) and w_* from h_i and $\overline{w'\theta'}_0$. Note that regional roughness length also can be estimated on the basis of past experience at a similar site (see e.g., Asanuma et al. (2000)) when there is no topographic data or a simpler method is required.

References

Abrams, M., 2000. The advanced spaceborne thermal emission and reflection radiometer (ASTER): data products for the high spatial resolution imager on NASA's Terra platform. Int. J. Rem. Sens., 21, 847-859.

André, J. C., Goutorbe, J.-P. and Perrier, A., 1986. HAPEX-MOBILHY: A hydrologic atmospheric experiment, for the study of water budget and evaporation flux at the climate scale. Bull. Am. Meteorol. Soc., 67, 138-144.

André, J. C., LaCarrere, P. and Mahrt, L. J., 1979. Sur la distribution verticale de l'humidite dans une couche limite convective. J. Rech. Atmos., 13, 135-146.

Asanuma, J., 1996. Turbulence Variance Characteristics in the Unstable Atmospheric Boundary Layer above Flat Pine Forest. Ph.D. Thesis, Cornell University, U.S.

Asanuma, J. and Brutsaert, W., 1999. Turbulence variance characteristics of temperature and humidity in the unstable atmospheric surface layer above a variable pine forest. Water Resour. Res., 35, 515-521.

Asanuma, J., Dias, N. L., Kustas, W. P. and Brutsaert, W., 2000. Observations of neutral profiles of wind speed and specific humidity above a gently rolling landscape. J. Meteorol. Soc. Jpn., 78, 719-730.

Berger, B. W., Davis, K. J., Yi, C., Bakwin, P. S. and Zhao, C. L., 2001. Long-term carbon dioxide fluxes from a very tower in a northern forest: flux measurement methodology. J. Atmos. Oceanic Technol., 18, 529-542

Betts, A. K. and Ball, J. H., 1994. Budget analysis of FIFE 1987 Sonde Data. J. Geophys. Res., 99, 3655-3666.

Brutsaert, W., 1982. Evaporation into the Atmosphere. D. Reidel, Dordrecht. 299pp.

Brutsaert, W. and Mawdsley, J. A., 1976. The applicability of planetary boundary layer theory to calculate regional evapotranspiration. Water Resour. Res., 12, 852-858.

1   Brutsaert, W. and Sugita, M., 1991. A bulk similarity approach in the atmospheric boundary layer using
2   radiometric skin temperature to determine regional surface fluxes.   Bound.-Layer Meteorol., 55, 1-23.

3   Caughey, S. and Palmer, S., 1979. Some aspects of turbulent structure through the depth of the convective
4   boundary layer. Q. J. R. Met. Soc., 105, 811-827.

5   Deardorff, J. W., 1970. Convective velocity and temperature scales for the unstable planetary boundary layer
6   and for Rayleigh convection. J. Atmos. Sci., 27, 1211-1213.

7   Driedonks, A. G. M., 1982. Models and observations of the growth of the atmospheric boundary layer.
8   Boundary-Layer Meteorol., 23, 283-306.

9   Eng, K., Coulter, R. L. and Brutsaert, W., 2003. Vertical velocity variance in the mixed layer from Radar
10   wind profilers.   J. Hydrologic Engrg., 8, 301-307.

11   Grant, A. L. M. and Mason, P. J., 1990. Observations of boundary layer structure over complex terrain. Quart.
12   J. Roy. Mereor. Soc., 116, 159-186.

13   Hiyama, T., Sugita, M. and Kotoda, K., 1996. Regional roughness parameters and momentum fluxes over a
14   complex area.   J. Appl. Meteor., 35, 2179-2190.

15   Kaimal, J. C. and Finnigan, J. J., 1994. Atmospheric Boundary Layer Flows. Oxford University Press, New
16   York. 289 pp.

17   Kaimal, J. C., Wyngaard, J. C., Haugan, D. A., Cote, O. R. and Izumi, Y., 1976. Turbulence structure in the
18   convective boundary layer.   J. Atmos. Sci., 33, 637-662.

19   Kalnay, E. Kanamitsu, M., Kistler, R., Collins, W., Deaven, D., Gandin, L., Iredell, M., Saha, S., White, G.,
20   Woollen, J., Zhu, Y., Leetmaa, A. and Reynolds, B., 1996. The NCEP/NCAR 40-year reanalysis project.
21   Bull. Amer. Meteor. Soc., 77, 437-471.

22   Katul, G., Hsieh, C.-I, Oren, R., Ellsworth, D. and Phillips, N., 1996. Latent and sensible heat flux
23   predictions from a uniform pine forest using surface renewal and flux variance methods.
24   Boundary-Layer Meteorol.,80, 249-282.

25   Kustas, W. P. and Brutsaert, W., 1986.   Wind profile constants in a neutral atmospheric boundary layer over
26   complex terrain.   Boundary-Layer Meteorol., 34, 35-54.

27   Kustas, W. P. and Brutsaert, W., 1987a. Virtual heat entrainment in the mixed layer over very rough terrain.
28   Boundary-Layer Meteorol., 38, 141-157.

29   Kustas, W. P. and Brutsaert, W., 1987b. Budget of water vapor in the unstable boundary layer over rugged
30   terrain. J. Clim. Appl., 607-620.

1   Lenschow, D. H. and Stankov, B. B., 1986. Length scale in the convective boundary layer. J. Atmos. Sci., 43,

2   1198-1209.

3   Lenschow, D. H., Mann, J. and Kristensen, L., 1994. How long is long enough when measuring fluxes and

4   other turbulence statistics? J. Atmos. Oceanic Technol., 11, 661-673.

5   Lenschow, D. H., Wyngaard, J. C. and Pennell, W. T., 1980. Mean-field and second-moment budgets in a

6   baroclinic, convective boundary layer.   J. Atmos. Sci., 37, 1313-1326.

7   Lettau, H., 1969. Note on aerodynamic roughness-parameter estimation on the basis of roughness-element

8   description.   J. Appl. Meteor., 8, 828-832.

9   Li, S-G.., Asanuma, J., Kotani, A., Eugster, W., Davaa, G., Oyunbaatar, D. and Sugita, M., 2005.   Net

10   ecosystem carbon dioxide exchange over grazed steppe in central Mongolia. Global Change Biology, 11,

11   1941-1955

12   Liu, X., and Ohtaki, E., 1997. An independent method to determine the height of the mixed layer.

13   Boundary-Layer Meteorol., 85, 497-504.

14   Moeng, C.-H. and Wyngaard, J.C., 1984. Statistics of conservative scalars in the convective boundary layer.

15   J. Atmos. Sci., 41, 3161-3169.

16   Raupach, M. R. and Finnigan, J. J., 1995. Scale issues in boundary-layer meteorology: Surface energy

17   balances in heterogeneous terrain.   Hydrol. Process., 9, 589-612.

18   Sato, T. and Kimura, F., 2005. Diurnal cycle of convective instability around the central mountains in Japan

19   during the warm season. J. Atmos. Sci., 62, 1626-1636.

20   Sato, T., Kimura, F. and Kitoh A., 2006. Projection of global warming onto regional precipitation over

21   Mongolia using a regional climate model.   J. Hydrol., this issue.

22   Sorbjan, Z., 1989. Structure of the Atmospheric Boundary Layer, Prentice Hall, New Jersey.

23   Stull, R. B., 1976. The energetics of entrainment across a density interface.   J. Atmos. Sci., 33, 1260 - 1267.

24   Stull, R. B., 1988. An Introduction to Boundary Layer Meteorology. Kluwer Academic Publishers, Dordrecht.

25   666pp.

26   Sugita, M. and Brutsaert, W., 1990. Wind velocity measurements in the neutral boundary layer above hilly

27   prairie. J. Geophys. Res., 95 (D6), 7617-7624.

28   Sugita, M., Endo, N. and Hiyama, T, 1999. Regional surface momentum flux derived from atmospheric

29   boundary layer bulk similarity approach.   J. Geophys. Res., 104 (D14), 16965-16972.

30   Sugita, M. and Kawakubo, N., 2003. Surface and mixed-layer variance methods to estimate regional sensible

heat flux at the surface.   Boundary-Layer Meteorol.,106,117-145.

Sugita, M., Asanuma, J., Tsujimura, M., Mariko, S., Lu M., Kimura, F., Azzaya, D. and Adyasuren Ts., 2006, An Overview of the Rangelands Atmosphere-Hydrosphere-Biosphere Interaction Study Experiment in Northeastern Asia (RAISE), J. Hydrol., this issue.

Sun and Marht, L., 1994. Spatial distribution of surface fluxes estimated from remotely sensed variables. J. Appl. Meteorol., 33, 1341-1353.

Tennekes, H., 1973. A model for the dynamics of the inversion above a convective boundary layer.   J. Atmos. Sci., 30, 558-567.

Twine, T.E., Kustas, W. P., Norman, J. M., Cook, D. R., Houser, P. R., Meyers, T. P., Prueger, J. H., Starks, P. J. and Wesely, M. L., 2000. Correcting eddy-covariance flux underestimates over a grassland.   Agric. For. Meteorol., 103, 279-300.

Weil, J. C. and Horst, T. W., 1992. Footprint estimates for atmospheric flux measurements in the convective boundary layer.   In: Schwarts, S.E. and Slinn, W. G. N. (Eds.), Precipitation Scavenging and Atmosphere-Surface Exchange, Vol.2, Hemisphere, Washington, DC, pp. 717-728.

Wesely, M. L., 1988. Use of variance techniques to measure dry air-surface exchange rates. Boundary-Layer Meteorol., 44, 13-31.

Willmott, C. J., 1981. On the validation of models. Phys. Geogr., 2, 184-194.

Wyngaard, J. C., 1985. Structure of the planetary boundary layer and implications for its modelling. J. Clim. Appl. Meteorol., 24, 1131-1142.

Wyngaard, J. C. and Brost, R. A., 1984. Top-down and buttom-up diffusion of a scalar in the convective boundary layer. J. Atmos. Sci., 41, 102-112.

Wyngaard, J. C., Coté, O. R. and Izumi, Y., 1971. Local free convection, similarity, and the budgets of shear stress and heat flux. J. Atmos. Sci., 28, 1171-1182.

Zilitinkevich, S. S., 1975. Resistance laws and prediction equations for the depth of the planetary boundary layer. J. Atmos. Sci., 32, 741-752.

1   Figure and table captions

2

3   Fig. 1

4   Study area. The bold lines represent flight segments, and circle indicates the ground based observation site at

5   KBU. The surface image and counter lines at 50 m interval are based on ASTER data products (Abrams,

6   2000).

7

8   Fig. 2

9   Power spectra fS for temperature fluctuation as a function of cyclic frequency f.   The thin solid lines, dashed

10   lines and dash and dot lines represent spectra for the flight level of around 200, 500 and 1000m respectively.

11   Solid thick line is the ensemble average of all lines.

12

13   Fig. 3

14   Vertical profile of the normalized variance of θ observed at grassland area (KBU). Open circles represent the

15   ground based measurements, and the closed circles indicate the aircraft measurements. Four functional lines

16   indicate the formulations (2), (3), (9) and (13).

17

18   Fig. 4

19   Comparison between the sensible heat fluxes $\overline{w'\theta'}_{vm}$ estimated with the variance methods based on

20   formulation (10) and $\overline{w'\theta'}_{s}$ observed on the ground by the eddy correlation method at the KBU flux site.

21   (a) (10) with the original constants, (b) (10) with calibrated constants, (c) (10) same as (b) but with additional

22   dimensionless variable parameters.   Squares in each panel indicate the points observed at elevation above

23   $0.5h_i$, and the circles are the others.

24

25   Fig. 5

26   Same as Figure 4 but for the variance formulation (11).

27

28   Fig. 6

29   Same as Figure 4 but for case i) of the variance formulation (12) with $v_h = v_0 = w_*$, entrainment model (4)

30   and the original constants, i.e., Eq. (12).   Open circles in panel (a) represent the result of (12) with $v_h = v_0 =$

1   w_* and the entrainment model (4), but the coefficients of Sugita and Kawakubo (2003) were used.

2

3   Fig. 7

4   Same as Figure 4 but for case ii) of the variance formulation (12) with $v_h = w_*$, $v_0 = v_*$, the entrainment model

5   (4) and the original constants.   Open circles of panel (a) represent the result of (12) with $v_h = w_*$, $v_0 = v_*$, and

6   the entrainment model (4), but the coefficients of Sugita and Kawakubo (2003) were used.

7

8   Fig. 8

9   Same as Figure 4 but for case iii) of the variance formulation (12) with $v_h = v_0 = v_*$ and the entrainment

10   model (8).   Open circles of panel (a) represent the result of (12) with $v_h = v_0 = v_*$, the entrainment model (8)

11   but the coefficients of Sugita and Kawakubo (2003) were used.

12

13   Fig. 9

14   A result of the sensitivity test and error propagation analysis.   The sensitivity of $\overline{w'\theta'}_{vm}$ to the change of

15   σ_θ^2 was evaluated by changing the value of σ_θ^2 for ± 0.1 K from 0.15K in the three cases, i) $v_0 = v_h = w_*$ with

16   (4), ii) $v_0 = v_*$, $v_h = w_*$ with (8), of (12) with the calibrated constants and for the condition of $\theta = 300$ K, $u_* =$

17   0.25 m s^{-1} and $\overline{w'\theta'}_s = 0.15$ K m s^{-1}.   The means of the resulting absolute changes of $\overline{w'\theta'}_{vm}$ for the ± 0.1

18   K change of σ_θ^2 are indicated.   The result of the error analysis (23) is also shown as the probable error of

19    $\overline{w'\theta'}_{vm}$ estimated by means of (22) with (10), (11), case i) of (12) and (14) with the calibrated constants and

20   for the condition of $\theta = 300$ K, $\sigma_\theta = 0.15$ K, $h_i = 1000$ m, $\delta\sigma_\theta = 0.1$K and $\delta\xi = 0.1$.

21

22

23   Fig. 10

24   Number of additional parameters and resulted rms (root mean square) difference between $\overline{w'\theta'}_s$ derived

25   form the eddy covariance method at the ground station, and $\overline{w'\theta'}_{vm}$ estimated by the variance methods.

26   The case of additional parameter zero is for (22) without additional parameters.   The variance formulation

27   (12) was used with $v_h = v_0 = w_*$.   The additional parameters, μ, v, β, and γ are expressed as Eqs. (17), (18),

28   (19) and (20), respectively. β_x, β_x and γ_x, γ_y are the x and y component of β and γ, respectively.

29

30

1   Table 1

2   Flight segment information with atmospheric conditions

3   MDST: Mongolian Daylight Saving Time (= local solar time + 2 hours), z: flight height (m), h_i: convective

4   boundary layer (CBL) height (m), H_s: sensible heat flux observed at the KBU station (W m^{-2}), T_*: CBL

5   temperature scale (K), w_*: CBL velocity scale (m s^{-1}), U: wind velocity (m s^{-1}), WD: wind direction (degree,

6   0º = northern wind), U and WD are the output of TERC-RAMS, at 800hPa (inside the CBL)

7

8   Table 2

9   List of constants in variance formulations

10   MW84: Moeng and Wyngaard (1984), SK03: Sugita and Kawakubo (2003), A96: Asanuma (1996), C/C:

11   Coefficients calibrated in this study, A/P: Coefficients calibrated in this study with additional parameters

12

13   Table 3

14   Statistics in the comparison of flux, $\overline{w'\theta'}_s$ derived form the eddy covariance method at the ground station,

15   and $\overline{w'\theta'}_{vm}$ estimated by the variance methods

16   MW84: Moeng and Wyngaard (1984), SK03: Sugita and Kawakubo (2003), A96: Asanuma (1996), C/C:

17   Coefficients calibrated in this study, A/P: Coefficients calibrated in this study with additional parameters, N:

18   number of data, rms: root mean square, a: intercept of regression line, b: slope of regression line

19   ($\overline{w'\theta'}_{vm} = a + b\overline{w'\theta'}_s$), $\overline{w'\theta'}_{vm}$: estimated flux by variance methods, $\overline{w'\theta'}_s$: observed flux at the KBU

20   station, d: index of agreement (Willmott, 1981), $\overline{w'\theta'}_s / \overline{w'\theta'}_{vm}$: ratio of the mean $\overline{w'\theta'}_s$ and $\overline{w'\theta'}_{vm}$

21

22   Table 4

23   List of parameters added to variance formulations

24   The additional parameters, ξ, μ, ν, β, and γ are expressed as Eqs. (16), (17), (18), (19) and (20), respectively.

1

2

3

4

5

6

7

8
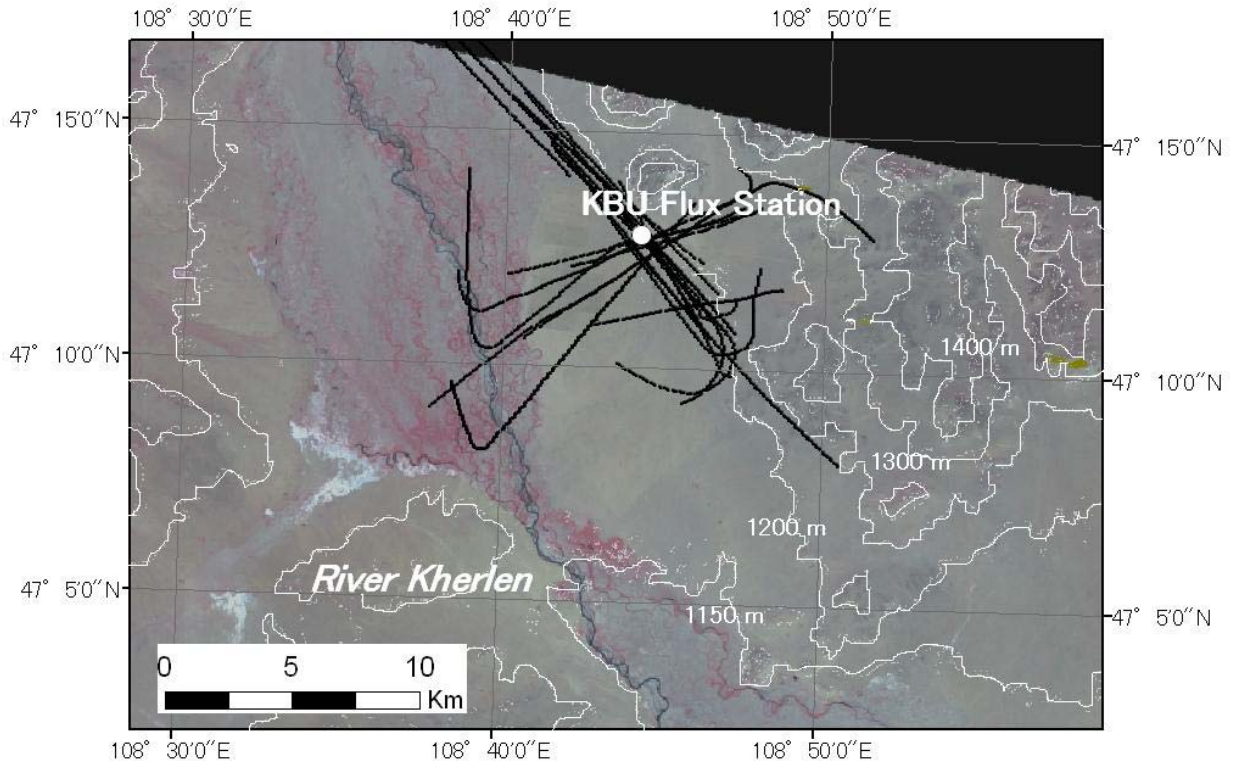
9

10

11

12

13

14

15

16   Fig. 1   Kotani and Sugita

Fig. 2   Kotani and Sugita
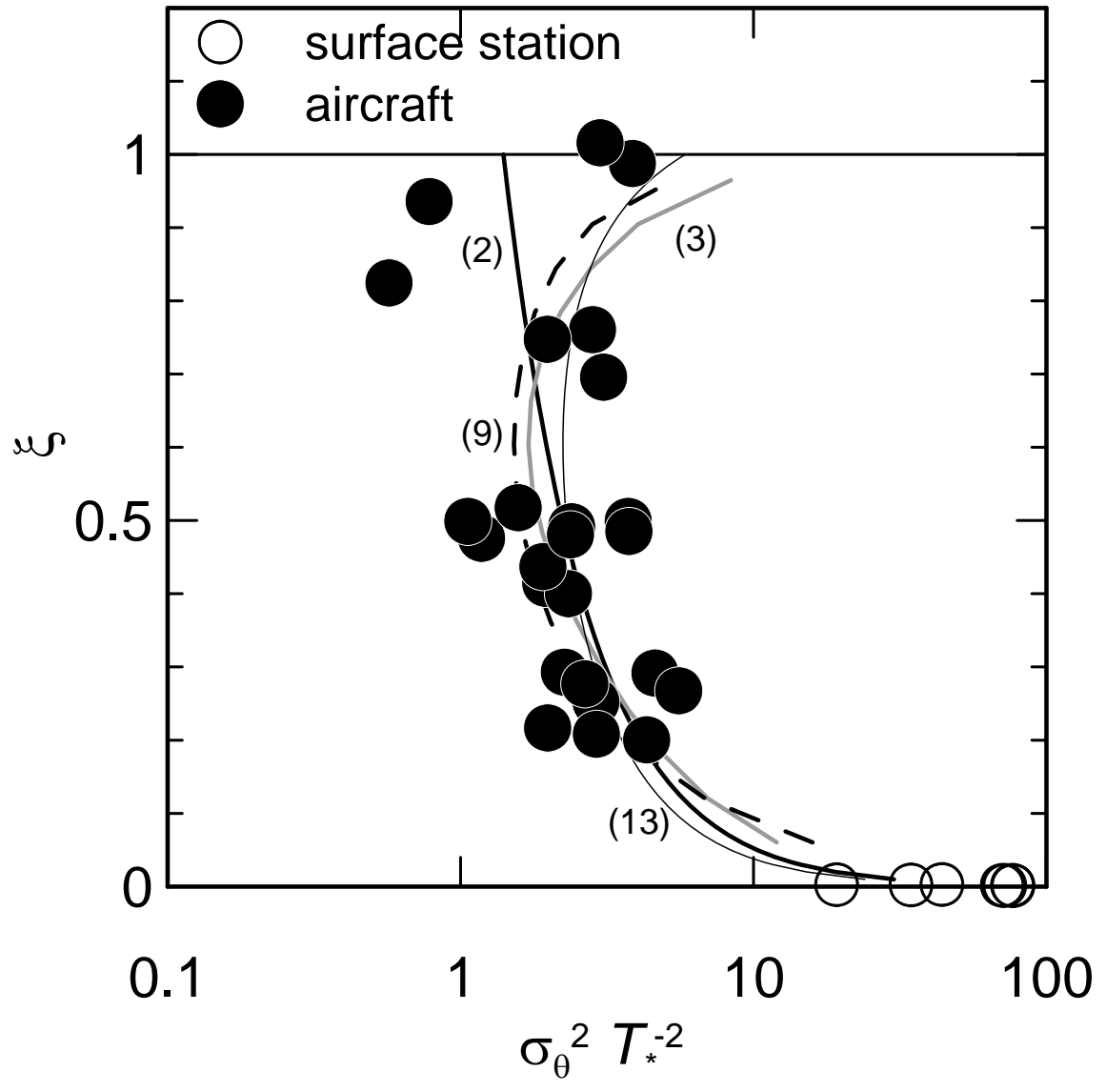
Fig. 3   Kotani and Sugita
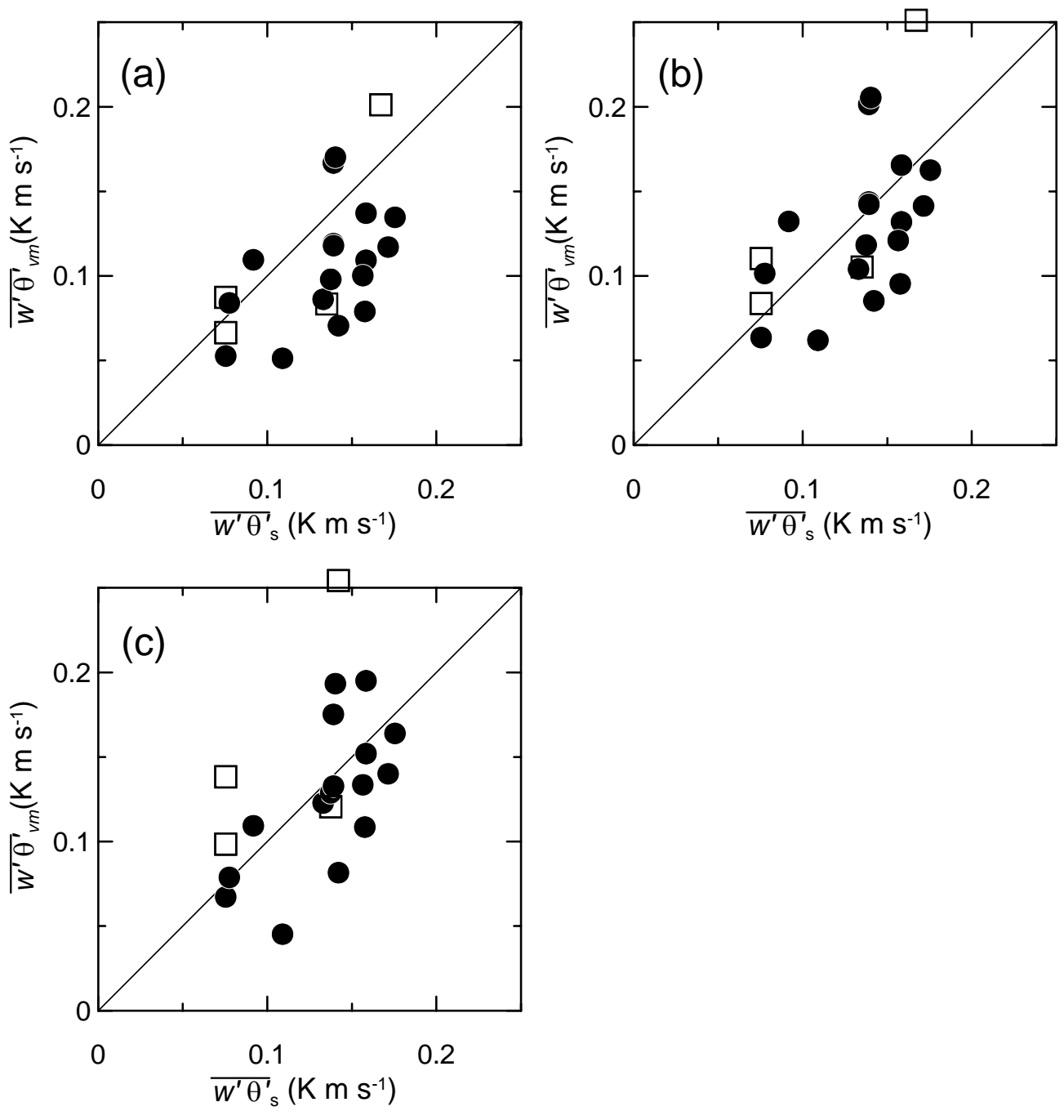
Fig. 4   Kotani and Sugita

1
2
3
4
5
6
7
8
9
10
11
12
13
14
15
16
17
18
19
20
21
22
23
24
25
26
27
28
29
30
31
32
33
34
35
36
37

Fig. 5   Kotani and Sugita

(a)

$\overline{w'\theta'}_{vm}$ (K m s^{-1})

$\overline{w'\theta'}_s$ (K m s^{-1})

(b)

$\overline{w'\theta'}_{vm}$ (K m s^{-1})

$\overline{w'\theta'}_s$ (K m s^{-1})

(c)

$\overline{w'\theta'}_{vm}$ (K m s^{-1})

$\overline{w'\theta'}_s$ (K m s^{-1})
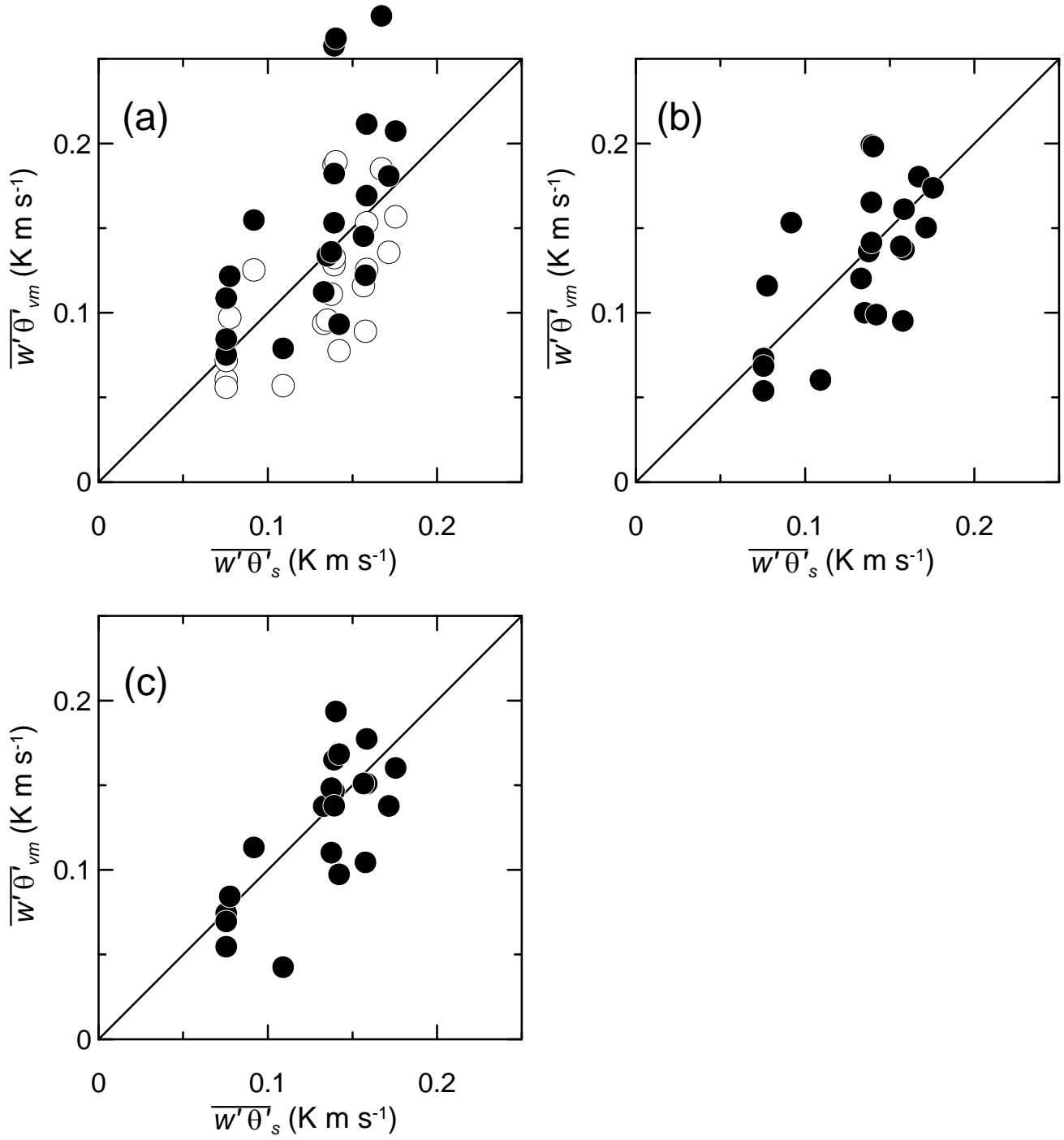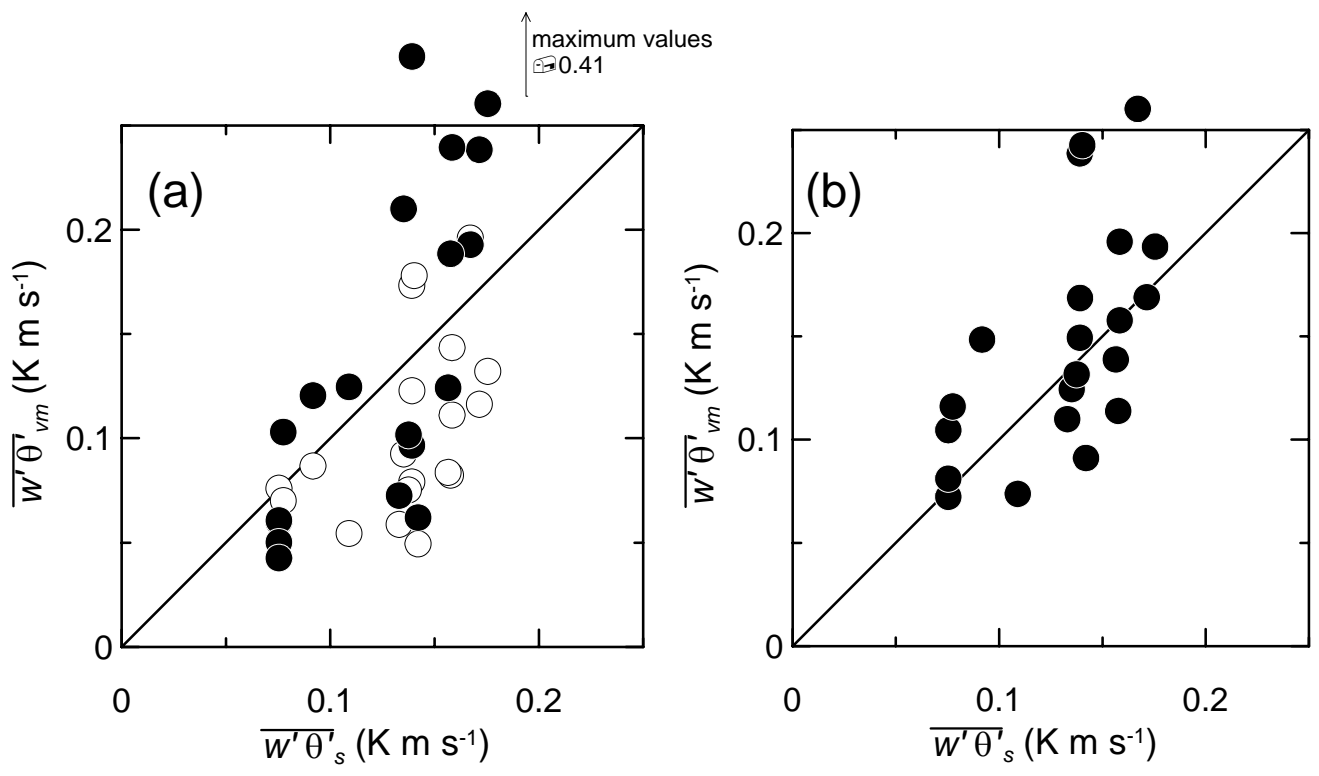
Fig. 6   Kotani and Sugita

1
2
3
4
5
6
7
8
9
10
11
12
13
14
15
16
17
18
19
20
21
22
23
24
25
26
27
28
29
30
31
32
33
34
35
36
37
38 Fig. 7   Kotani and Sugita
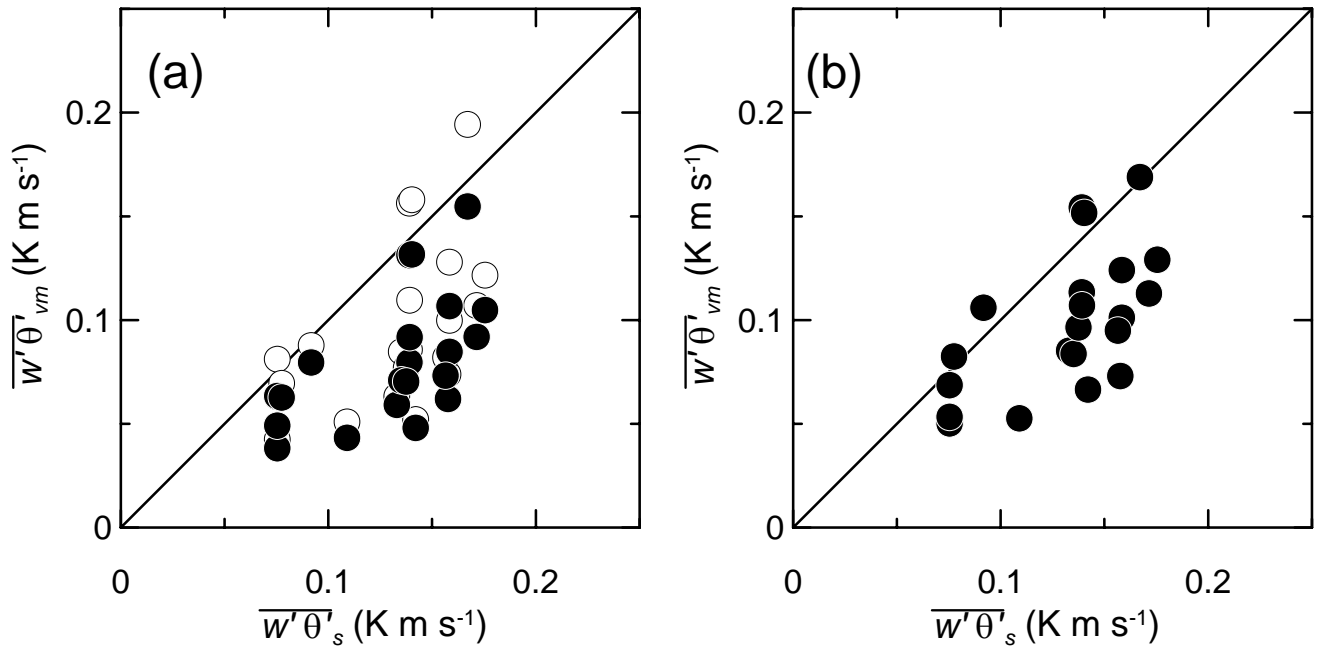
Fig. 8   Kotani and Sugita

Fig. 9   Kotani and Sugita
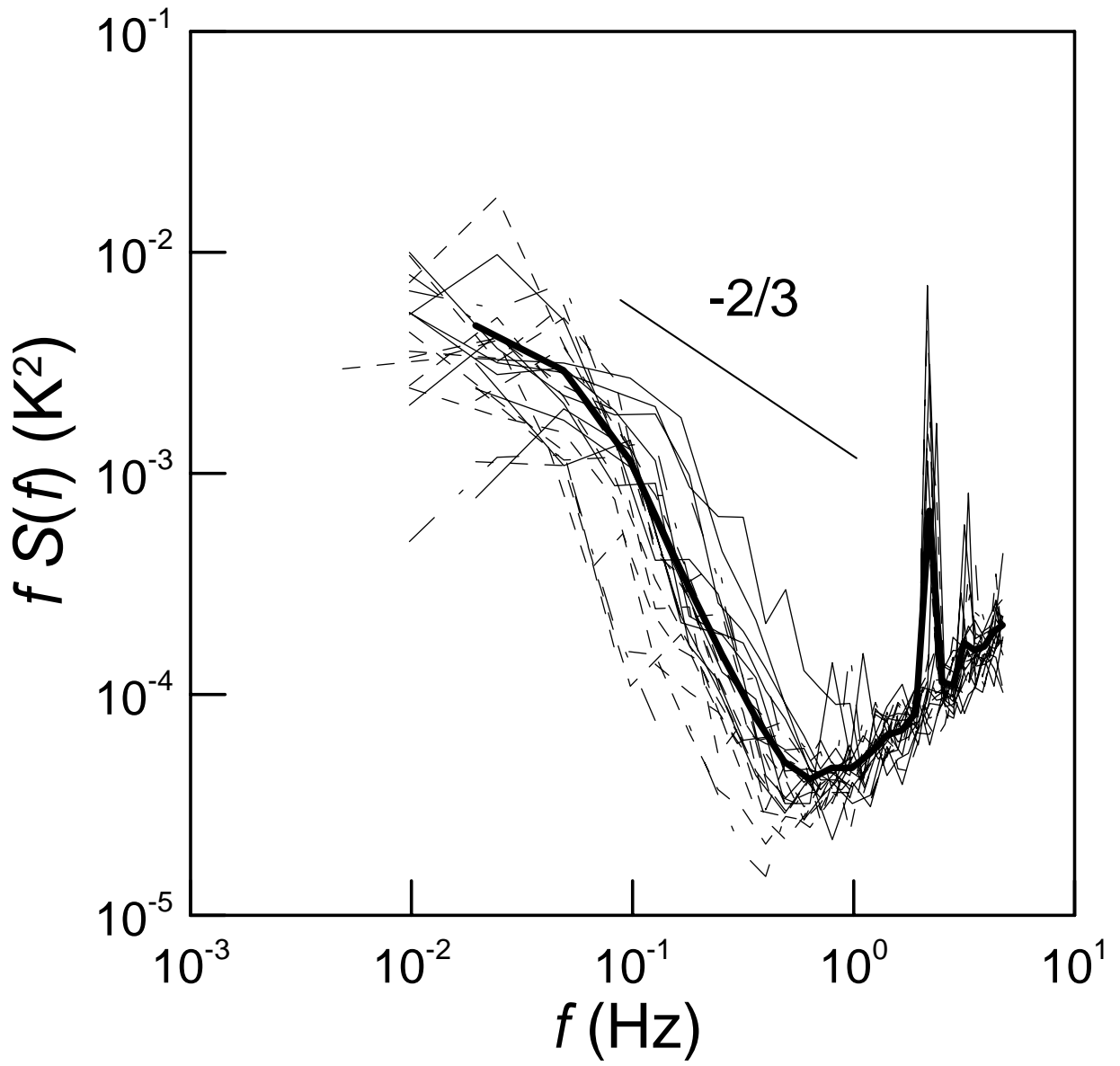
41

Fig. 10   Kotani and Sugita

1
2
3
4
5
6
7
8
9
10
11
12
13
14
15
16
17
18
19
20
21
22
23
24
25
26
27
28
29
30
31
32
33
34
35
36
37
38

Legend:
- (10) $\delta\sigma_\theta$
- (10) $\delta\xi$
- (10) δP
- (11) $\delta\sigma_\theta$
- (11) $\delta\xi$
- (11) δP
- (12) $\delta\sigma_\theta$
- (12) $\delta\xi$
- (12) δP
- (14) $\delta\sigma_\theta$
- (14) $\delta\xi$
- (14) δP

y-axis: ξ (1, 0.5, 0)

x-axis: $\delta\overline{w'\theta'}_s$ (K m s^{-1}), 0, 0.1, 0.2, 0.3
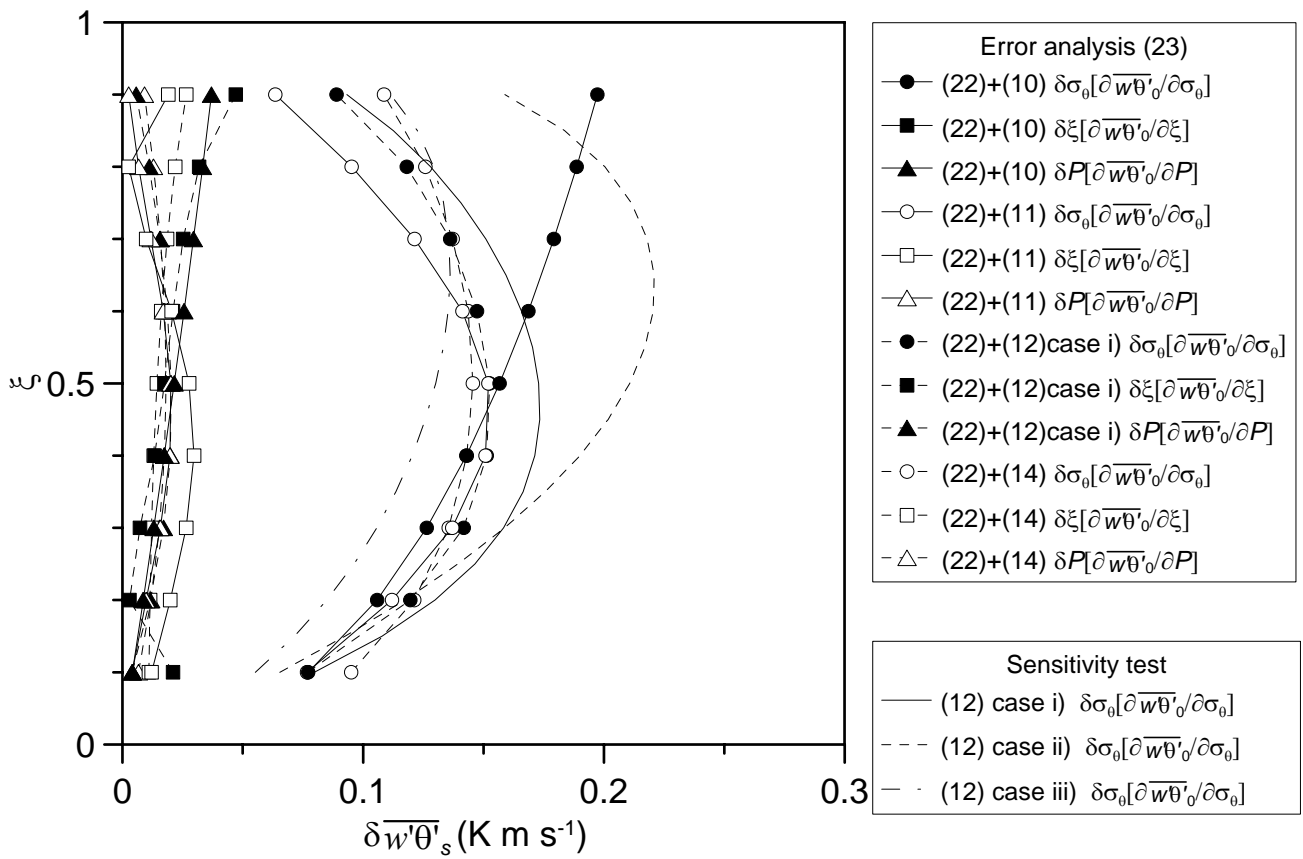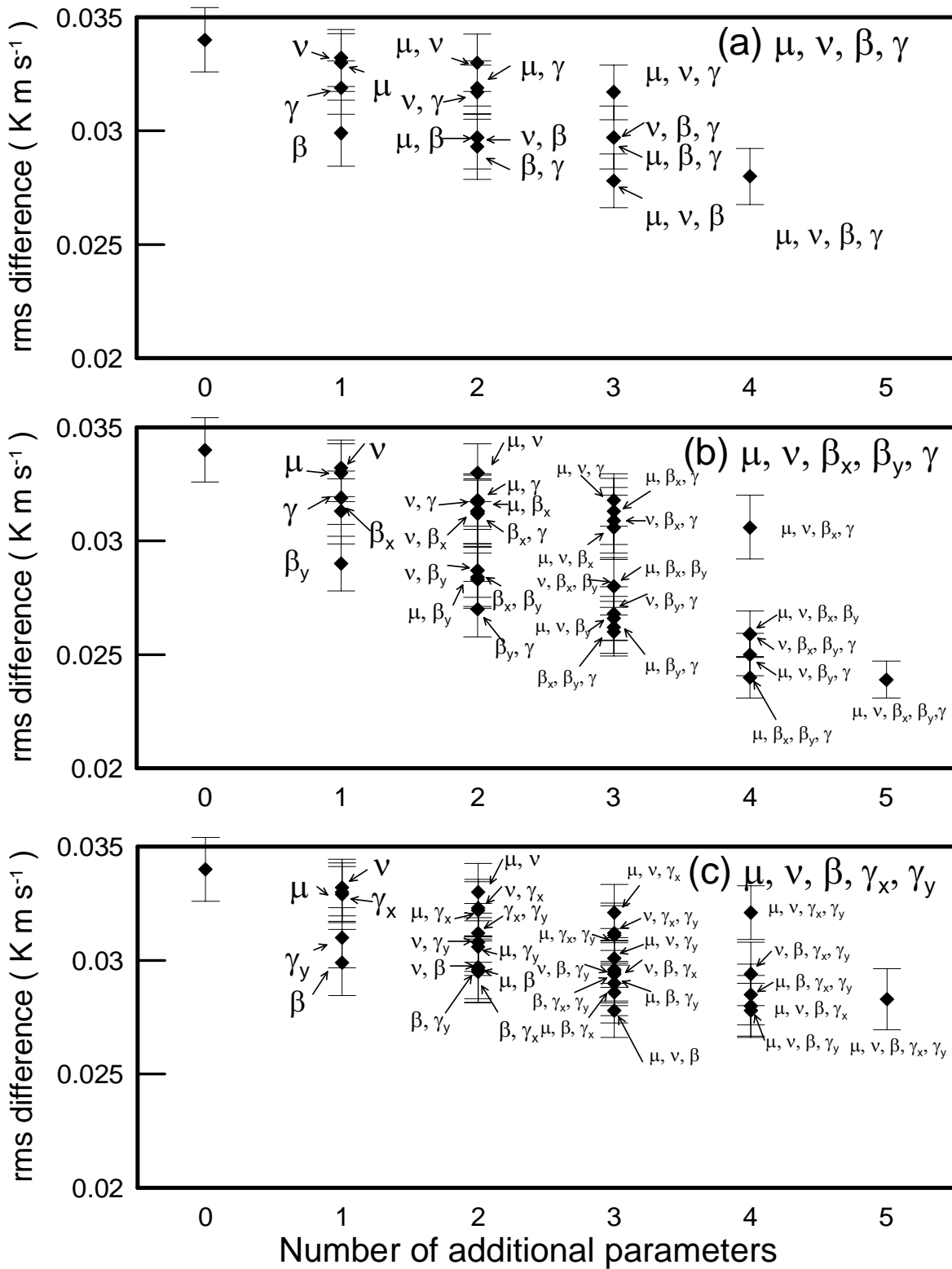
Fig. 11　Kotani and Sugita

Table 1 Flight segment information with atmospheric conditions

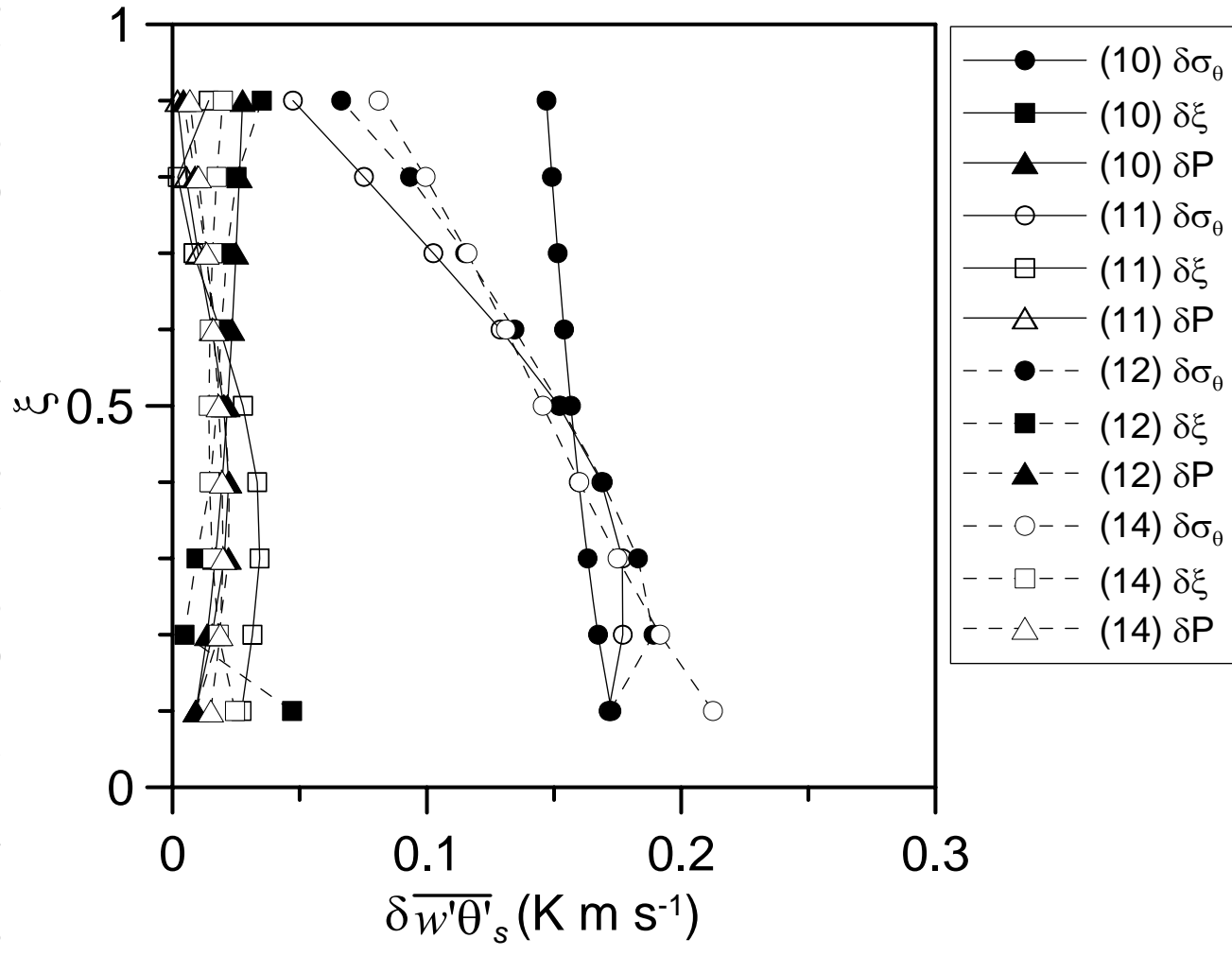| Date (2003)	Segment name	Time (MDST) (HHMM)	Segment length (km)	z (m)	h_i (m)	z/h_i	H_s (W m^{-2})	T_* (K)	w_* (m s^{-1})	U (m s^{-1})	WD (deg)	weather condition
July 19	200-KBU500	1541	9.31	437	900	0.49	139	0.088	1.6	7.2	265	clear
	200-KBU200	1549	8.80	180		0.20	139	0.088	1.6	7.2	265	
July 20	201-KBU200	1036	7.48	194	700	0.28	77	0.063	1.2	1.8	315	clear/ cloudy
	201-KBU500a	1045	7.23	532		0.76	77	0.063	1.2	1.8	316	
	201-KBU500b	1053	7.84	523		0.75	77	0.063	1.2	1.7	316	
July 23	204-KBU1000	1236	11.21	914	900	1.02	123	0.085	1.6	6.6	85	clear
	204-KBU200	1254	10.13	187		0.21	123	0.085	1.6	6.5	85	
Aug. 21	233-KBU200a	1227	9.50	224	770	0.29	82	0.062	1.3	6.1	328	clear/ cloudy
	233-KBU200b	1234	10.03	206		0.27	97	0.069	1.3	6.2	328	
	233-KBU300	1241	7.52	384		0.50	116	0.078	1.4	6.2	327	
Aug. 22	234-KBU1000	1233	7.68	1062	1075	0.99	134	0.078	1.6	3.1	24	generally clear
	234-KBU500b	1251	7.89	556		0.52	142	0.081	1.7	3.1	35	
	234-KBU200	1256	8.19	271		0.25	144	0.082	1.7	3.1	38	
Aug. 23	235-KBU1000	1225	7.56	1123	1200	0.94	148	0.080	1.8	1.7	16	generally clear
	235-KBU500a	1231	11.73	577		0.48	147	0.079	1.8	1.5	17	
	235-KBU500b	1239	11.98	599		0.50	148	0.080	1.8	1.2	18	
	235-KBU200	1253	5.24	260		0.22	150	0.080	1.8	0.7	22	
Oct. 2	276-KBU1000	1245	11.59	1113	1600	0.70	189	0.080	2.1	8.2	3	generally clear
	276-KBU500a	1255	11.01	662		0.41	194	0.081	2.1	8.1	3	
	276-KBU500c	1304	11.50	640		0.40	198	0.083	2.1	8.1	2	
Oct. 3	277-KBU1000	1255	19.87	1072	1300	0.82	184	0.085	1.9	2.5	302	generally clear
	277-KBU500a	1307	7.24	568		0.44	176	0.083	1.9	2.4	304	
	277-KBU500b	1309	12.66	639		0.49	176	0.083	1.9	2.4	305	
	277-KBU500c	1318	11.12	618		0.48	175	0.083	1.9	2.3	307	
	277-KBU200	1323	8.93	381		0.29	174	0.082	1.9	2.3	309	

MDST: Mongolian Daylight Saving Time (= local solar time + 2 hours), z: flight height (m), h_i: convective boundary layer (CBL) height (m), H_s: sensible heat flux observed at the KBU station (W m^{-2}), T_*: CBL temperature scale (K), w_*: CBL velocity scale (m s^{-1}), U: wind velocity (m s^{-1}), WD: wind direction (degree, 0° = northern wind), U and WD are the output of TERC-RAMS, at 800hPa (inside the CBL)

Table 2　List of constants in variance formulations

(a) Eqs. (2)

variance formulation	z/h_i	a
Kaimal et al. (1976)		1.8
C/C	< 0.5	1.4
C/C	< 0.8	1.5

(b) Eqs. (3)

variance formulation	A_θ	D	$C_{M\theta_0}$	$C_{M\theta_i}$
Sorbjan (1989)	0.2	0	2	8
C/C	0.2	0	1.6	18.0

(c) Eqs. (7)

variance formulation				a_1	a_2	a_3	a_4	a_5	a_6	a_7
	v_0	v_h								
MW84	w_*	w_*	(4) with $A_\theta = 0.2$	14	-2/3	1	–	–	0.47	-5/4
SK03	w_*	w_*	(4) with $A_\theta = 0.2$	25.0	-2/3	0.91	–	–	0.53	-5/4
C/C	w_*	w_*	(4) with $A_\theta = 0.2$	28.0	-2/3	0.31	-1/3	-5/8	0.33	-5/4
A96	v_*	w_*	(4) with $A_\theta = 0.2$	38.3	-3/2	8.01	-3/4	-5/8	2.04	-5/4
SK03	v_*	w_*	(4) with $A_\theta = 0.2$	45.0	-2/3	6.00	-1/3	-5/8	1.89	-5/4
C/C	v_*	w_*	(4) with $A_\theta = 0.2$	11.2	-2/3	0	-3/4	-5/8	0.45	-5/4
A96	v_*	v_*	(8) with $A = 0.2$, B=5	2.58	-3/2	3.3	0	0	1.04	-5/4
SK03	v_*	v_*	(8) with $A = 0.2$, B=5	10.71	-2/3	0	-1/3	-5/8	1.05	-5/4
C/C	v_*	v_*	(8) with $A = 0.2$, B=5	5.8	-2/3	3.0	-1/3	-5/8	0.29	-5/4

(d) Eq. (13)

variance formulation	b_1	b_2	b_3	b_4
–	0.9	0.7	1.2	-1.2

(e) Eq. (21)

variance formulation				c_1	c_2	c_3	c_4	c_5	c_6	c_7	c_8	c_9
$F(z/h_i)$	v_0	v_h										
(2)	–	–	$z/h_i < 0.5$	27.2	-2	-1.2	-3	765.3	-2	-8.1	-1	0.0
(2)	–	–	$z/h_i < 0.8$	549.3	-1	-1.8	-3	41.0	-1	176.4	-3	0.0
(3)	–	–	–	18.7	-1	-0.9	-3	704.6	-2	-4.0	-1	-0.1
(7)	w_*	w_*	(4) with $A_\theta = 0.2$	16.3	-1	-0.8	-3	688.2	-2	-15.9	-2	-0.1
(13)	–	–	–	305.9	-2	-0.7	-3	661.3	-2	-40.2	-3	-0.2

MW84: Moeng and Wyngaard (1984), SK03: Sugita and Kawakubo (2003), A96: Asanuma (1996), C/C: Coefficients calibrated in this study

1 Table 3 Statistics in the comparison of flux, $\overline{w'\theta'}_s$ derived form the eddy covariance method at the

2 ground station, and $\overline{w'\theta'}_{vm}$ estimated by the variance methods

3

4 (a) Eq. (10)

variance formulation	z/h_i	N	rms difference (K m s^{-1})	a	b	d	$\overline{w'\theta'}_s/\overline{w'\theta'}_{vm}$
Kaimal et al. (1976)	< 0.5	17	0.044	0.034	0.53	0.59	0.78
C/C	< 0.5	17	0.038	0.043	0.64	0.65	0.95
A/P	< 0.5	17	0.032	0.003	0.92	0.99	0.94
Kaimal et al. (1976)	< 0.8	21	0.042	0.024	0.64	0.67	0.82
C/C	< 0.8	21	0.039	0.028	0.73	0.70	0.94
A/P	< 0.8	21	0.034	0.023	0.78	0.74	0.96

5

6 (b) Eq. (11)

variance formulation	N	rms difference (K m s^{-1})	a	b	d	$\overline{w'\theta'}_s/\overline{w'\theta'}_{vm}$
Sorbjan (1989)	21	0.043	0.009	0.97	0.70	1.04
C/C	21	0.034	0.013	0.84	0.77	0.95
A/P	21	0.029	-0.01	1.02	0.84	0.95

7

8 (c) Eq. (12)

	v_0	v_h	entrainment model	N	rms difference (K m s^{-1})	a	b	d	$\overline{w'\theta'}_s/\overline{w'\theta'}_{vm}$
MW84	w_*	w_*	(4) with $A_\theta = 0.2$	21	0.053	0.014	1.07	0.63	1.19
SK03	w_*	w_*	(4) with $A_\theta = 0.2$	21	0.036	0.014	0.78	0.75	0.89
C/C	w_*	w_*	(4) with $A_\theta = 0.2$	21	0.034	0.023	0.81	0.77	0.98
A/P	w_*	w_*	(4) with $A_\theta = 0.2$	21	0.027	0.001	0.95	0.83	0.95
A96	v_*	w_*	(4) with $A_\theta = 0.2$	21	0.107	-0.071	1.89	0.42	1.35
SK03	v_*	w_*	(4) with $A_\theta = 0.2$	21	0.049	0.002	0.74	0.64	0.76
C/C	v_*	w_*	(4) with $A_\theta = 0.2$	21	0.046	0.018	0.98	0.68	1.12
A96	v_*	v_*	(8) with $A = 0.2, B = 5$	21	0.058	0.012	0.52	0.55	0.61
SK03	v_*	v_*	(8) with $A = 0.2, B = 5$	21	0.050	0.013	0.62	0.61	0.72
C/C	v_*	v_*	(8) with $A = 0.2, B = 5$	21	0.044	0.019	0.61	0.66	0.75

9

1   (d) Eq. (14)

variance formulation	N	rms difference (K m s^{-1})	a	b	d	$\overline{w'\theta'}_s / \overline{w'\theta'}_{vm}$
C/C	21	0.034	0.026	0.75	0.77	0.95
A/P	21	0.029	-0.001	0.97	0.83	0.96

2

3   MW84: Moeng and Wyngaard (1984), SK03: Sugita and Kawakubo (2003), A96: Asanuma (1996), C/C:

4   Coefficients calibrated in this study, A/P: Coefficients calibrated in this study with additional parameters, N:

5   number of data, rms: root mean square, a: intercept of regression line, b: slope of regression line ($\overline{w'\theta'}_{vm} = a +$

6    $b\,\overline{w'\theta'}_s$), $\overline{w'\theta'}_{vm}$: estimated flux by variance methods, $\overline{w'\theta'}_s$: observed flux at the KBU station, d: index of

7   agreement (Willmott, 1981), $\overline{w'\theta'}_s / \overline{w'\theta'}_{vm}$: ratio of the mean $\overline{w'\theta'}_s$ and $\overline{w'\theta'}_{vm}$

Table 4 List of parameters added to variance formulations

Date (2003)	Segment name	ξ	$|\mu|$	ν	β	β_x	β_y	γ	γ_x	γ_y
July 19	200-KBU500	0.49	529.4	1.1	22.9	22.4	4.4	64.3	28.1	-57.8
	200-KBU200	0.20	552.4	1.1	23.7	23.3	4.6	64.3	28.1	-57.8
July 20	201-KBU200	0.28	218.9	1.3	42.8	33.1	-27.1	38.9	29.3	-25.6
	201-KBU500a	0.76	218.8	1.3	42.8	33.1	-27.1	38.9	29.3	-25.6
	201-KBU500b	0.75	219.0	1.2	42.2	32.7	-26.8	38.9	29.3	-25.6
July 23	204-KBU1000	1.02	109.6	1.0	57.6	45.1	-35.8	122.9	-120.8	-22.8
	204-KBU200	0.21	111.8	1.0	59.4	46.6	-36.9	122.9	-120.8	-22.8
Aug. 23	233-KBU200a	0.29	16.7	0.8	18.3	10.5	14.9	18.7	-18.7	-0.3
	233-KBU200b	0.27	18.7	0.8	17.2	9.9	14.0	15.8	-15.8	-0.3
	233-KBU300	0.50	21.2	0.8	17.0	9.8	13.9	13.3	-13.3	-0.2
Aug. 24	234-KBU1000	0.99	18.9	0.9	50.4	30.1	-40.4	68.8	1.3	-68.7
	234-KBU500b	0.52	19.7	0.9	49.2	29.4	-39.5	65.0	1.3	-65.0
	234-KBU200	0.25	19.9	0.8	48.6	29.1	-39.0	63.9	1.2	-63.8
Aug. 25	235-KBU1000	0.94	28.8	1.2	141.3	125.2	-65.7	63.1	-42.1	46.9
	235-KBU500a	0.48	28.8	1.2	142.1	125.8	-66.0	63.4	-42.4	47.2
	235-KBU500b	0.50	28.8	1.2	140.9	124.8	-65.4	62.9	-42.0	46.8
	235-KBU200	0.22	29.1	1.2	139.8	123.8	-64.9	62.1	-41.5	46.2
Oct. 2	276-KBU1000	0.70	62.9	1.4	37.6	25.9	-27.2	15.1	14.9	-2.6
	276-KBU500a	0.41	64.0	1.4	37.3	25.7	-27.0	14.7	14.5	-2.5
	276-KBU500c	0.40	65.5	1.4	37.0	25.6	-26.8	14.4	14.2	-2.4
Oct. 3	277-KBU1000	0.82	62.4	1.1	89.6	76.9	-46.0	46.0	-19.5	-41.6
	277-KBU500a	0.44	60.6	1.2	91.0	78.1	-46.7	47.9	-20.4	-43.3
	277-KBU500b	0.49	60.4	1.2	90.1	77.4	-46.3	47.9	-20.4	-43.3
	277-KBU500c	0.48	60.6	1.2	90.7	77.9	-46.6	48.1	-20.4	-43.5
	277-KBU200	0.29	60.1	1.2	90.7	77.8	-46.5	48.5	-20.6	-43.9

The additional parameters, ξ, μ, ν, β, and γ are expressed as Eqs. (16), (17), (18), (19) and (20), respectively.